NAVAL POSTGRADUATE SCHOOL

Monterey, California

THESIS

A LINEAR SYSTEMS THEORY APPROACH TO THE RANGE-INDEPENDENT ACOUSTIC CHANNEL

by

Luiz Alberto Lopes de Souza

June 1989

Thesis Advisor Lawrence J. Ziomek

Unclassified

security classification of this page

REPORT DOCUMENTATION PAGE

1a Report Security Classification Unclassified			1b Restrictive Markings
2a Security Classification Authority			3 Distribution Availability of Report
2b Declassification Downgrading Schedule			Approved for public release; distribution is unlimited.
4 Performing Organization Report Number(s)			5 Monitoring Organization Report Number(s)
6a Name of Performing Organization Naval Postgraduate School	6b Office Symbol *(if applicable)* 33		7a Name of Monitoring Organization Naval Postgraduate School
6c Address *(city, state, and ZIP code)* Monterey, CA 93943-5000			7b Address *(city, state, and ZIP code)* Monterey, CA 93943-5000
8a Name of Funding Sponsoring Organization	8b Office Symbol *(if applicable)*		9 Procurement Instrument Identification Number
8c Address *(city, state, and ZIP code)*			10 Source of Funding Numbers
			Program Element No / Project No / Task No / Work Unit Accession No

11 Title *(Include security classification)* A LINEAR SYSTEMS THEORY APPROACH TO THE RANGE-INDEPENDENT ACOUSTIC CHANNEL

12 Personal Author(s) Luiz Alberto Lopes de Souza

13a Type of Report	13b Time Covered	14 Date of Report *(year, month, day)*	15 Page Count
Master's Thesis	From To	June 1989	105

16 Supplementary Notation The views expressed in this thesis are those of the author and do not reflect the official policy or position of the Department of Defense or the U.S. Government.

17 Cosati Codes			18 Subject Terms *(continue on reverse if necessary and identify by block number)*
Field	Group	Subgroup	underwater acoustics,medium transfer function,Pekeris waveguide,waveform prediction,linear systems

19 Abstract *(continue on reverse if necessary and identify by block number)*

Using linear systems theory as a framework, the solution for the acoustic field present ia a range-independent acoustic channel excited by a complex-weighted, planar array of point sources with an arbitrary input electrical signal is derived. The ocean medium is characterized by a transfer function, obtainable as the solution to the Helmholtz wave equation. The unbounded homogeneous medium equations are derived as a special case of the waveguide problem. The problem of interference due to the presence of a pressure-release surface is also derived as a special case. The linear systems approach lends itself to a modular computer implementation, in which different ocean medium models are represented by subroutines implementing their transfer functions. The equations for a range-independent medium are implemented as a group of subprograms. Results are presented for the special cases of a homogeneous medium and the surface reflection problem, which can be checked against known, easily interpreted analytical solutions. Finally, an example of waveform prediction for the isospeed, three-layer waveguide is presented.

20 Distribution Availability of Abstract	21 Abstract Security Classification	
☒ unclassified unlimited ☐ same as report ☐ DTIC users	Unclassified	
22a Name of Responsible Individual Lawrence J. Ziomek	22b Telephone *(include Area code)* (408) 646-3206	22c Office Symbol 62Zm

DD FORM 1473,84 MAR 83 APR edition may be used until exhausted
All other editions are obsolete

security classification of this page

Unclassified

Approved for public release; distribution is unlimited

A Linear Systems Theory Approach to the Range-Independent Acoustic Channel

by

Luiz Alberto Lopes de Souza
Lieutenant Commander, Brazilian Navy
B.S., General Roberto Lisboa Engineering College, Rio de Janeiro, 1979

Submitted in partial fulfillment of the
requirements for the degrees of

MASTER OF SCIENCE IN ELECTRICAL ENGINEERING

and

MASTER OF SCIENCE IN ENGINEERING ACOUSTICS

from the

NAVAL POSTGRADUATE SCHOOL
June 1989

Author: _____
Luiz Alberto Lopes de Souza

Approved By: _____
Lawrence J. Ziomek, Thesis Advisor

_____
James H. Miller, Second Reader

_____
John P. Powers, Chairman, Department of Electrical and Computer Engineering

_____
Anthony A. Atchley, Chairman, Engineering Acoustics Academic Committee

_____
Gordon E. Schacher, Dean of Science and Engineering

ABSTRACT

Using linear systems theory as a framework, the solution for the acoustic field present in a range-independent acoustic channel excited by a complex-weighted, planar array of point sources with an arbitrary input electrical signal is derived. The ocean medium is characterized by a transfer function, obtainable as the solution to the Helmholtz wave equation. The transfer function for an isospeed, three-layer waveguide is derived. The unbounded homogeneous medium equations are derived as a special case of the waveguide problem. The problem of interference due to the presence of a pressure-release surface is also derived as a special case. The linear systems approach lends itself to a modular computer implementation, in which different ocean medium models are represented by subroutines implementing their transfer functions. The equations for a range-independent medium are implemented as a group of subprograms. Results are presented for the special cases of a homogeneous medium and the surface reflection problem, which can be checked against known, easily interpreted analytical solutions. Finally, an example of waveform prediction for the isospeed, three-layer waveguide is presented.

TABLE OF CONTENTS

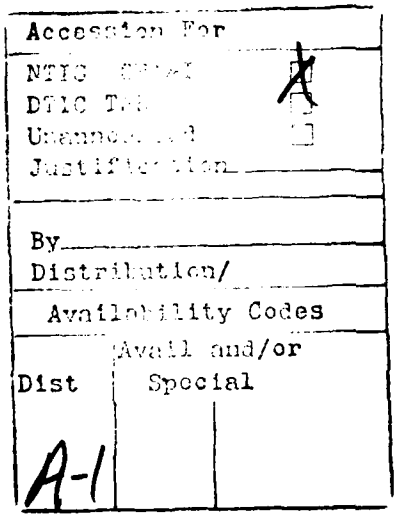

I. INTRODUCTION

Model-based or matched-field signal processing refers to the use of the knowledge of the physics of a problem for the construction of mathematical models and its application to suitable signal processing algorithms. Its application to underwater acoustics has been the subject of many papers in the signal processing literature, as in Ziomek and Blount [Ref. 1], Baggeroer, Kuperman and Schmidt [Ref. 2] and references therein. As the interest in this field grows and new algorithms are developed, so will the need for simulation tools to verify the behavior of those algorithms. Such tools should be able to generate signals with spatial and temporal structures like those found in real environments.

The waveform prediction problem has been studied by Officer [Ref. 3:pp. *101-110,130] for the specific cases of pulse reflection* from a boundary and transmission in shallow water. DiNapoli and Deavenport [Ref.4:pp. 131-134] describe briefly a method employing the Fast-Field-Program (FFP) suitable to range-independent problems. Our purpose is to derive a generic solution for the range-independent, time-invariant, deterministic acoustic channel excited by an array of point sources transmitting an arbitrary signal. In our derivation we will use a linear systems approach to the acoustic problem, as described in Ziomek [Ref. 5], whose notation we follow closely. In particular, we will apply our results to the isospeed Pekeris waveguide. As we will show, the linear systems approach lends itself to a modular computer implementation, where different ocean media are represented by subroutines or functions implementing their transfer function.

In Section II we present the basic input-output relationships for a space-variant, time-independent linear system, which are the basis of our derivations. Next, we show how those equations can be used to represent an acoustic channel. The particular case of a range-independent ocean is then studied, when we derive the output waveform equation and describe the process of derivation of the medium transfer function. Finally, we apply the above results to the isospeed Pekeris waveguide. In Section III we discuss computer implementation issues and present some results of a computer implementation of the Pekeris waveguide equations.

II. ANALYSIS

A. THE ACOUSTIC CHANNEL AS A LINEAR SYSTEM

In this section we will present some results from the theory of space-time linear systems [Ref. 5], establish the notation to be used, and derive some intermediate results to be used in subsequent sections.

1. Space-Variant, Time-Invariant Linear Systems

a. Impulse Response

Linear, time-invariant, space-variant filters, as shown in Fig. 1, are represented by linear partial differential equations whose coefficients are time independent. In linear systems terminology, such systems are characterized by their time-invariant, space-dependent impulse response $h(\tau,\mathbf{r}_0;\mathbf{r})$. The output $\varphi(t,\mathbf{r})$ is given by [Ref. 5:p. 8]

$$\varphi(t,\mathbf{r}) = \int_{-\infty}^{\infty}\int_{-\infty}^{\infty} g(t-\tau,\mathbf{r}-\mathbf{r}_0)\, h(\tau,\mathbf{r}_0;\mathbf{r})\, d\tau\, d\mathbf{r}_0 . \tag{1}$$

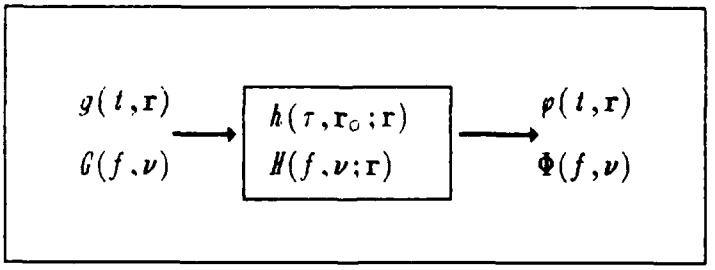

Fig. 1. A Linear, Time-Invariant, Space-Variant System

A physical interpretation of h, τ and $\mathbf{r}_o$ can be obtained by letting the input be an impulse applied at time $t = t_o$ and at position $\mathbf{r} = \mathbf{r}_s$, that is, $g(t,\mathbf{r}) = \delta(t-t_o,\mathbf{r}-\mathbf{r}_s) = \delta(t-t_o)\ \delta(\mathbf{r}-\mathbf{r}_s)$. Substituting this expression for $g(t,\mathbf{r})$ into Eq. (1) and using the sifting property of the impulse function we obtain, for the output,

$$\varphi(t,\mathbf{r}) = h(\underbrace{t-t_o}_{\tau}, \underbrace{\mathbf{r}-\mathbf{r}_s}_{\mathbf{r}_o}; \mathbf{r}), \tag{2}$$

from which we can define $h(\tau,\mathbf{r}_o;\mathbf{r})$ as the response of the system at time t and position $\mathbf{r}$ due to the application of an impulse τ seconds ago, that is, at the instant $t_o = t-\tau$, when the point source is positioned at $\mathbf{r}_s = \mathbf{r}-\mathbf{r}_o$. Figure 2 illustrates the geometry of this problem.

b. Transfer Function

Let the input to the system be a plane wave, that is, $g(t,\mathbf{r}) = e^{j2\pi(f_o t-\boldsymbol{\nu}_o\cdot\mathbf{r})}$, with frequency f_o and spatial frequency vector $\boldsymbol{\nu}_o$. The output of the system is given by Eq. (1) as

$$\varphi(t,\mathbf{r}) = \int_{-\infty}^{\infty}\int_{-\infty}^{\infty} e^{j2\pi(f_o t-\boldsymbol{\nu}_o\cdot\mathbf{r})}\, e^{-j2\pi(f_o\tau-\boldsymbol{\nu}_o\cdot\mathbf{r}_o)}\, h(\tau,\mathbf{r}_o;\mathbf{r})\, d\tau\, d\mathbf{r}_o, \tag{3a}$$

$$\varphi(t,\mathbf{r}) = e^{j2\pi(f_o t-\boldsymbol{\nu}_o\cdot\mathbf{r})} \int_{-\infty}^{\infty}\int_{-\infty}^{\infty} e^{-j2\pi(f_o\tau-\boldsymbol{\nu}_o\cdot\mathbf{r}_o)}\, h(\tau,\mathbf{r}_o;\mathbf{r})\, d\tau\, d\mathbf{r}_o, \tag{3b}$$

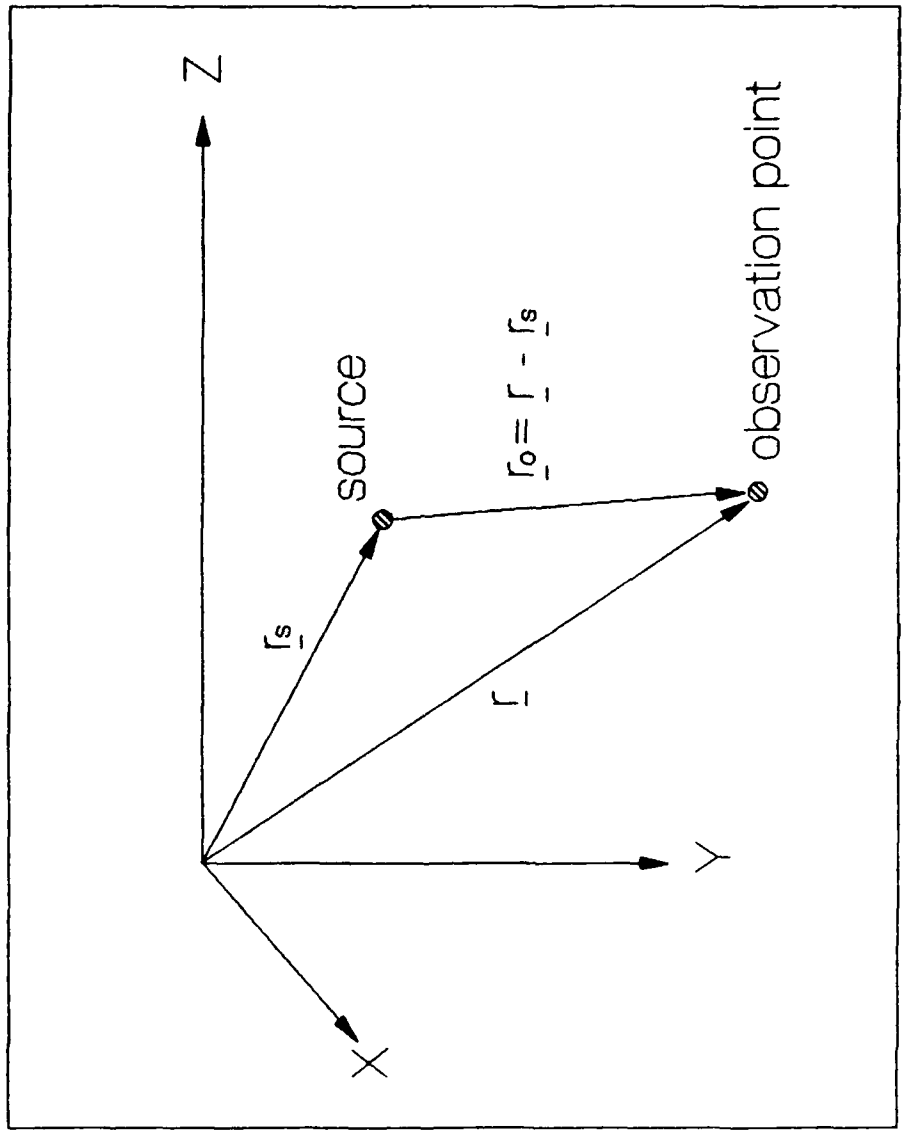

Fig. 2. Basic Geometry for the Interpretation of $h(\tau, r_s, r)$

or

$$\varphi(t,\mathbf{r}) = e^{j2\pi(f_o t - \boldsymbol{\nu}_o \cdot \mathbf{r})}\, \mathfrak{F}_{\tau-f}\mathfrak{F}_{\mathbf{r}_o-\boldsymbol{\nu}}\{\, h(\tau,\mathbf{r}_o;\mathbf{r})\,\}\Big|_{\substack{f=f_o \\ \boldsymbol{\nu}=\boldsymbol{\nu}_o}} \tag{3c}$$

where $\mathfrak{F}_{\tau-f}$ represents the *time-domain Fourier transform* and $\mathfrak{F}_{\mathbf{r}_o-\boldsymbol{\nu}}$ represents the *spatial-domain Fourier transform*. The subscripts under the symbol $\mathfrak{F}$ represent the variables involved in each transform. We define $H(f,\boldsymbol{\nu};\mathbf{r})$, the system transfer function, as follows:

$$H(f,\boldsymbol{\nu};\mathbf{r}) \triangleq \mathfrak{F}_{\tau-f}\mathfrak{F}_{\mathbf{r}_o-\boldsymbol{\nu}}\{\, h(\tau,\mathbf{r}_o;\mathbf{r})\,\} = \int_{-\infty}^{\infty}\int_{-\infty}^{\infty} e^{-j2\pi(f\tau - \boldsymbol{\nu}\cdot\mathbf{r}_o)}\, h(\tau,\mathbf{r}_o;\mathbf{r})\, d\tau\, d\mathbf{r}_o\,. \tag{4}$$

Using this definition, the output of the system can be written as

$$\varphi(t,\mathbf{r}) = H(f_o,\boldsymbol{\nu}_o;\mathbf{r})\; e^{j2\pi(f_o t - \boldsymbol{\nu}_o\cdot\mathbf{r})}\,, \tag{5}$$

the expected result from linear systems theory.

The parameter $\mathbf{r}_o$ in the integrations in Eqs. (1) and (4) represents the vectorial difference between the observation point $\mathbf{r}$ and the point source position $\mathbf{r}_s$. The integrations must be performed taking $\mathbf{r}$ as a constant, that is, by changing the source position $\mathbf{r}_s$ so that $\mathbf{r}_o$ assumes all possible values in R^3, and the results, $\varphi(t,\mathbf{r})$ or $H(f_o,\boldsymbol{\nu}_o;\mathbf{r})$, are valid for that "fixed" observation point $\mathbf{r}$.

c. *Response to a Time-Harmonic Point Source*

When evaluating the transfer function, it is convenient to use a time-harmonic point source as the input, $g(t,\mathbf{r}) = e^{j2\pi f_o t}\,\delta(\mathbf{r}-\mathbf{r}_s)$ with frequency f_o and location $\mathbf{r}_s$. The output, from Eqs. (1) and (4), is given by

$$\varphi(t,\mathbf{r}) = \int_{-\infty}^{\infty}\int_{-\infty}^{\infty} e^{j2\pi f_o(t-\tau)}\,\delta(\mathbf{r}-\mathbf{r}_s-\mathbf{r}_o)\,h(\tau,\mathbf{r}_o;\mathbf{r})\,d\tau\,d\mathbf{r}_o\,, \tag{6a}$$

$$\varphi(t,\mathbf{r}) = e^{j2\pi f_o t}\int_{-\infty}^{\infty} e^{-j2\pi f_o \tau}\,h(\tau,\mathbf{r}-\mathbf{r}_s;\mathbf{r})\,d\tau\,. \tag{6b}$$

$$\varphi(t,\mathbf{r}) = e^{j2\pi f_o t}\,\mathfrak{F}_{\tau-f}\{\,h(\tau,\mathbf{r}_o;\mathbf{r})\,\}\Big|_{\substack{f=f_o\\ \mathbf{r}_o=\mathbf{r}-\mathbf{r}_s}}\,, \tag{6c}$$

or

$$\varphi(t,\mathbf{r}) = e^{j2\pi f_o t}\,\mathfrak{F}^{-1}_{\mathbf{r}_o-\nu}\{\,H(f_o,\nu_o;\mathbf{r})\,\}\,. \tag{6d}$$

d. *Transform Relationships*

(1) Fourier Transform Definitions and Notation. The time-domain Fourier transform of a function $g(t,\mathbf{r}) = g(t,x,y,z)$ and its inverse are given, respectively, by

$$G(f,\mathbf{r}) = \mathfrak{F}_{t-f}\{\,g(t,\mathbf{r})\,\} = \int_{-\infty}^{\infty} g(t,\mathbf{r})\,e^{-j2\pi f t}dt\,, \tag{7}$$

and

$$g(t,\mathbf{r}) = \mathfrak{F}^{-1}_{t-f}\{\, G(f,\mathbf{r}) \,\} = \int_{-\infty}^{\infty} G(f,\mathbf{r})\; e^{j2\pi f t} df. \tag{8}$$

The spatial Fourier transform and its inverse are given, respectively, by

$$G(t,\boldsymbol{\nu}) = \mathfrak{F}_{\mathbf{r}-\boldsymbol{\nu}}\{\, g(t,\mathbf{r}) \,\} = \int_{-\infty}^{\infty} g(t,\mathbf{r})\; e^{j2\pi\boldsymbol{\nu}\cdot\mathbf{r}} d\mathbf{r}\,, \tag{9}$$

and

$$g(t,\mathbf{r}) = \mathfrak{F}^{-1}_{\mathbf{r}-\boldsymbol{\nu}}\{\, G(t,\boldsymbol{\nu}) \,\} = \int_{-\infty}^{\infty} G(t,\boldsymbol{\nu})\; e^{-j2\pi\boldsymbol{\nu}\cdot\mathbf{r}} d\boldsymbol{\nu}\,, \tag{10}$$

where $d\mathbf{r} = dx\, dy\, dz$, $d\boldsymbol{\nu} = df_x\, df_y\, df_z$, and $\boldsymbol{\nu}\cdot\mathbf{r} = xf_x + yf_y + zf_z$. The above transforms involve triple integrals and can be split into three spatial transforms in x (f_x), y (f_y) and z (f_z). For example, the transforms in x (f_x) are written as

$$G(t,f_x,y,z) = \mathfrak{F}_{x-f_x}\{\, g(t,x,y,z) \,\} = \int_{-\infty}^{\infty} g(t,x,y,z)\; e^{j2\pi f_x x} dx\,, \tag{11}$$

and

$$g(t,x,y,z) = \mathfrak{F}^{-1}_{x-f_x}\{\, G(t,f_x,y,z) \,\} = \int_{-\infty}^{\infty} G(t,f_x,y,z)\; e^{-j2\pi f_x x} df_x\,. \tag{12}$$

The transforms in y (f_y) and z (f_z) follow the same notation. The full space-time transforms can be written as

$$G(f,\boldsymbol{\nu}) = \mathfrak{F}_{t-f}\mathfrak{F}_{\mathbf{r}-\boldsymbol{\nu}}\{\, g(t,\mathbf{r})\,\} = \mathfrak{F}_{t-f}\mathfrak{F}_{x-f_x}\,\mathfrak{F}_{y-f_y}\,\mathfrak{F}_{z-f_z}\{\, g(t,\mathbf{r})\,\}\,, \tag{13a}$$

or

$$G(f,\boldsymbol{\nu}) = \int_{-\infty}^{\infty}\int_{-\infty}^{\infty} e^{-j2\pi(f\,t-\boldsymbol{\nu}\cdot\mathbf{r})}\, g(t,\mathbf{r})\, dt\, d\mathbf{r}\,, \tag{13b}$$

and

$$g(t,\mathbf{r}) = \mathfrak{F}^{-1}_{t-f}\mathfrak{F}^{-1}_{\mathbf{r}-\boldsymbol{\nu}}\{\, G(f,\boldsymbol{\nu})\,\} = \mathfrak{F}^{-1}_{t-f}\mathfrak{F}^{-1}_{x-f_x}\,\mathfrak{F}^{-1}_{y-f_y}\,\mathfrak{F}^{-1}_{z-f_z}\{\, G(f,\boldsymbol{\nu})\,\}\,, \tag{14a}$$

or

$$g(t,\mathbf{r}) = \int_{-\infty}^{\infty}\int_{-\infty}^{\infty} e^{j2\pi(f\,t-\boldsymbol{\nu}\cdot\mathbf{r})}\, G(f,\boldsymbol{\nu})\, df\, d\boldsymbol{\nu}\,. \tag{14b}$$

The above relationships are valid for the impulse response/transfer function pair if t is replaced by τ and $\mathbf{r}$ is replaced by $\mathbf{r}_o = (x_o, y_o, z_o)$, that is,

$$H(f,\mathbf{r}_o;\mathbf{r}) = \mathfrak{F}_{\tau-f}\{\, h(\tau,\mathbf{r}_o;\mathbf{r})\,\}\,, \tag{15}$$

$$H(t,\boldsymbol{\nu};\mathbf{r}) = \mathfrak{F}_{\mathbf{r}_o-\boldsymbol{\nu}}\{\, h(\tau,\mathbf{r}_o;\mathbf{r})\,\}\,, \tag{16}$$

$$H(t,f_x,y_o,z_o;\mathbf{r}) = \mathfrak{F}_{x_o-f_x}\{\, h(\tau,x_o,y_o,z_o;\mathbf{r}) \,\}\,, \tag{17}$$

and

$$H(f,\boldsymbol{\nu};\mathbf{r}) = \mathfrak{F}_{\tau-f}\mathfrak{F}_{\mathbf{r}_o-\boldsymbol{\nu}}\{\, h(\tau,\mathbf{r}_o;\mathbf{r}) \,\}\,. \tag{4}$$

The same applies for the respective inverse transforms.

(2) Input-Output Relationships. During our developments, we will need to express the output of the system, $\varphi(t,\mathbf{r})$, in terms of the transformed input function $G(f,\boldsymbol{\nu})$ and the transfer function. From the Fourier transform definition

$$g(t,\mathbf{r}) = \int_{-\infty}^{\infty}\int_{-\infty}^{\infty} e^{j2\pi(ft-\boldsymbol{\nu}\cdot\mathbf{r})}\, G(f,\boldsymbol{\nu})\, df\, d\boldsymbol{\nu}\,, \tag{18}$$

follows the transform property

$$g(t-\tau,\mathbf{r}-\mathbf{r}_o) = \int_{-\infty}^{\infty}\int_{-\infty}^{\infty} e^{j2\pi(ft-\boldsymbol{\nu}\cdot\mathbf{r})}\, e^{-j2\pi(f\tau-\boldsymbol{\nu}\cdot\mathbf{r}_o)} G(f,\boldsymbol{\nu})\, df\, d\boldsymbol{\nu}\,. \tag{19}$$

Substituting this expression into Eq. (1) yields

$$\varphi(t,\mathbf{r}) = \int_{-\infty}^{\infty}\int_{-\infty}^{\infty}\int_{-\infty}^{\infty}\int_{-\infty}^{\infty} e^{j2\pi(ft-\boldsymbol{\nu}\cdot\mathbf{r})}\, e^{-j2\pi(f\tau-\boldsymbol{\nu}\cdot\mathbf{r}_o)}\, G(f,\boldsymbol{\nu}) \times h(\tau,\mathbf{r}_o;\mathbf{r})\, df\, d\boldsymbol{\nu}\, d\tau\, d\mathbf{r}_o\,, \tag{20a}$$

$$\varphi(t,\mathbf{r}) = \int_{-\infty}^{\infty}\int_{-\infty}^{\infty} e^{j2\pi(ft-\boldsymbol{\nu}\cdot\mathbf{r})} G(f,\boldsymbol{\nu}) \underbrace{\int_{-\infty}^{\infty}\int_{-\infty}^{\infty} h(\tau,\mathbf{r}_o;\mathbf{r})\ e^{-j2\pi(f\tau-\boldsymbol{\nu}\cdot\mathbf{r}_o)} d\tau\ d\mathbf{r}_o}_{H(f,\boldsymbol{\nu};\mathbf{r})} df\, d\boldsymbol{\nu}, \quad (20b)$$

or

$$\varphi(t,\mathbf{r}) = \int_{-\infty}^{\infty}\int_{-\infty}^{\infty} G(f,\boldsymbol{\nu})\ H(f,\boldsymbol{\nu};\mathbf{r})\ e^{j2\pi(ft-\boldsymbol{\nu}\cdot\mathbf{r})} df\, d\boldsymbol{\nu}\,, \quad (20c)$$

which is the desired relationship.

Analogous to a time-variant system, for which the frequencies at the output are different from the input, a space-variant system causes the output spatial frequency vector to be different from the input. We will use $\boldsymbol{\beta}$ to represent the output spatial frequency vector. The input-output relationship in the transformed form can be obtained by substituting Eq. (20c) into the Fourier transform definition

$$\Phi(f,\boldsymbol{\beta}) = \int_{-\infty}^{\infty}\int_{-\infty}^{\infty} \{\ \varphi(t,\mathbf{r})\ \}\ e^{-j2\pi(ft-\boldsymbol{\beta}\cdot\mathbf{r})} dt\, d\mathbf{r}\,. \quad (21)$$

Doing so yields

$$\Phi(f,\boldsymbol{\beta}) = \int_{-\infty}^{\infty}\int_{-\infty}^{\infty}\int_{-\infty}^{\infty}\int_{-\infty}^{\infty} G(\eta,\boldsymbol{\nu})\ H(\eta,\boldsymbol{\nu};\mathbf{r})\ e^{j2\pi(\eta t-\boldsymbol{\nu}\cdot\mathbf{r})} d\eta\, d\boldsymbol{\nu}\ e^{-j2\pi(ft-\boldsymbol{\beta}\cdot\mathbf{r})} dt\, d\mathbf{r}, \quad (22a)$$

$$\Phi(f,\boldsymbol{\beta}) = \int_{-\infty}^{\infty}\int_{-\infty}^{\infty}\int_{-\infty}^{\infty} G(\eta,\boldsymbol{\nu})\ H(\eta,\boldsymbol{\nu};\mathbf{r})\ e^{-j2\pi(\boldsymbol{\nu}-\boldsymbol{\beta})\cdot\mathbf{r}} \left\{\int_{-\infty}^{\infty} e^{-j2\pi(f-\eta)t} dt\right\} d\eta\, d\mathbf{r}\, d\boldsymbol{\nu}, \quad (22b)$$

$$\Phi(f,\beta) = \int_{-\infty}^{\infty}\int_{-\infty}^{\infty}\left\{\int_{-\infty}^{\infty} G(\eta,\nu)\, H(\eta,\nu;\mathrm{r})\, e^{-j2\pi(\nu-\beta)\cdot\mathrm{r}}\, \delta(f-\eta)\, d\eta\right\} d\mathrm{r}\, d\nu, \quad (22c)$$

$$\Phi(f,\beta) = \int_{-\infty}^{\infty}\int_{-\infty}^{\infty} G(f,\nu)\, H(f,\nu;\mathrm{r})\, e^{-j2\pi(\nu-\beta)\cdot\mathrm{r}}\, d\mathrm{r}\, d\nu\,. \quad (22d)$$

2. The Acoustic Channel

As long as we deal with small-amplitude acoustic signals, the governing wave equation is linear. We will restrict ourselves to time-invariant problems, where the properties of the medium do not change with time, and the source, receiver and the boundaries are motionless.

Figure 3 is a pictorial representation of the acoustic channel. A source or transmitter rectangular array "couples" an electrical signal to the medium and a receiver array transforms the acoustic signal back to electrical form. Both arrays are assumed to act as linear filters. We will not be concerned here with the generation of the electrical transmitted signal, assumed given, nor with the processing done on the received electrical signals at each hydrophone position. The acoustic channel can be represented by the block diagram shown in Fig. 1, which can be broken down into the three basic components sketched in Fig. 3: transmitter array, medium and receiver array. Figure 4 shows these components in block diagram form. [Ref. 5;pp. 3-4]

a. The medium

The propagation of the acoustic signal through the medium is governed by the wave equation

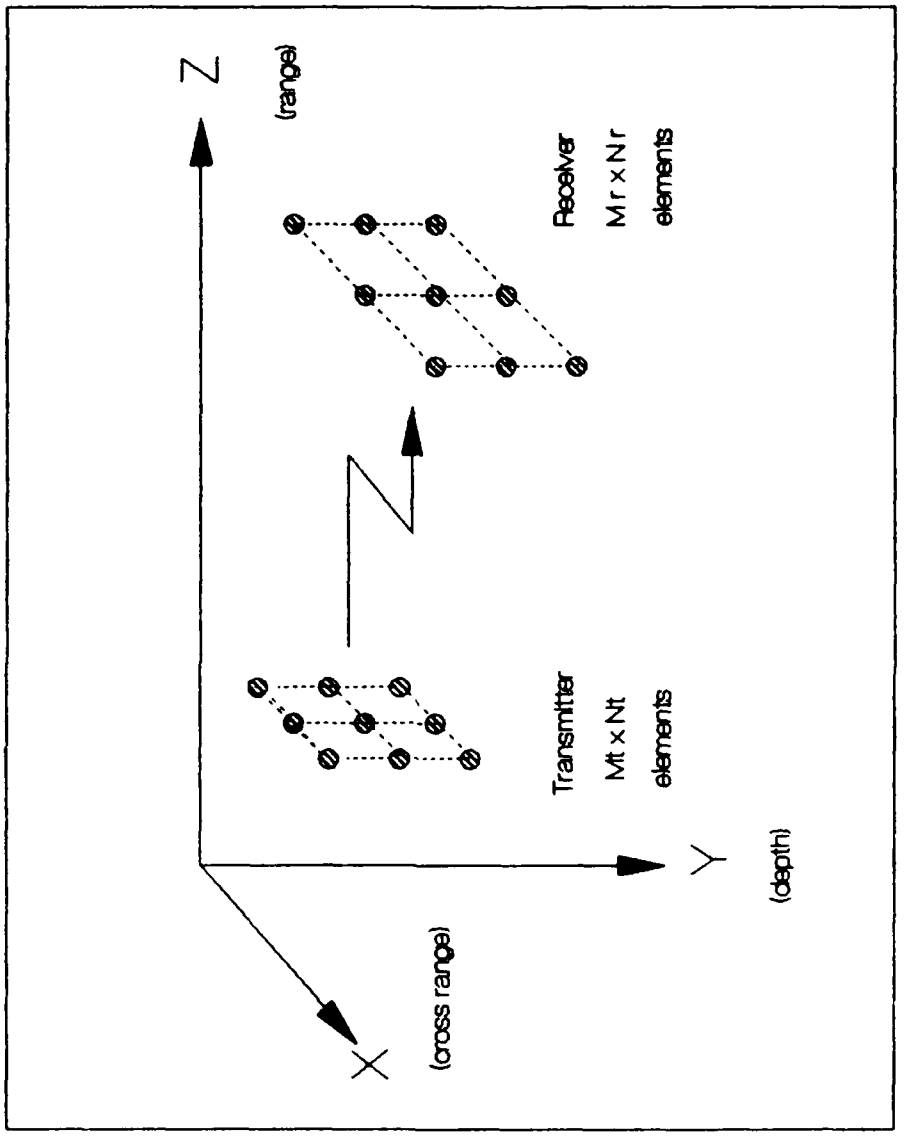

Fig. 3. Geometry of the Acoustic Channel Problem.

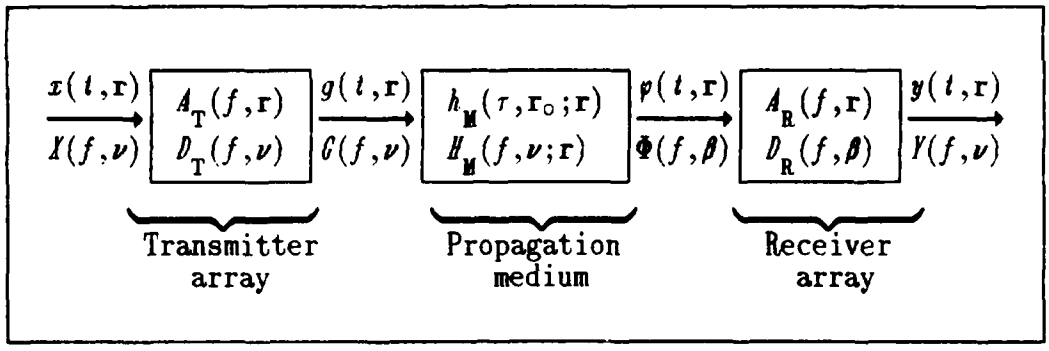

Fig. 4. Block-Diagram Representation of the Acoustic Channel.

$$\nabla^2 \varphi(t,\mathbf{r}) - \frac{1}{c^2(\mathbf{r})} \frac{\partial^2}{\partial t^2} \varphi(t,\mathbf{r}) = g(t,\mathbf{r}) \tag{23}$$

and appropriate boundary conditions, where $\varphi(t,\mathbf{r})$ is the velocity potential ($m^2 s^{-1}$), $g(t,\mathbf{r})$ is the source term, which represents the rate of mass injection into the space per unit mass or rate at which fluid volume is added per unit volume (s^{-1}) [Ref. 5;p. 1]. These two terms are represented in Fig. 4 as the output and input to the acoustic medium block, respectively. The solution of Eq. (23) is obtained from Eqs. (1) or (20c) as

$$\varphi(t,\mathbf{r}) = \int_{-\infty}^{\infty}\int_{-\infty}^{\infty} g(t-\tau,\mathbf{r}-\mathbf{r}_o)\, h_M(\tau,\mathbf{r}_o;\mathbf{r})\, d\tau\, d\mathbf{r}_o , \tag{24}$$

or

$$\varphi(t,\mathbf{r}) = \int_{-\infty}^{\infty}\int_{-\infty}^{\infty} G(f,\nu)\, H_M(f,\nu;\mathbf{r})\, e^{j2\pi(ft-\nu\cdot\mathbf{r})} df\, d\nu . \tag{25}$$

The transform of the output $\Phi(f,\beta)$ is a function of the spatial frequency vector β, which is, in general, different from ν, due to the space-variant nature of the medium. The physical meaning, in terms of ray acoustics, is that a non-homogeneous medium (H is a function of r) causes change in the direction of propagation of the sound.

The input-output relationship in the transformed form can be obtained from Eq. (22d), resulting in

$$\Phi(f,\beta) = \int_{-\infty}^{\infty}\int_{-\infty}^{\infty} G(f,\nu)\, H_{M}(f,\nu;\mathrm{r})\, e^{-j2\pi(\nu-\beta)\cdot\mathrm{r}}\, d\mathrm{r}\, d\nu\,. \tag{26}$$

If the system is space-invariant, an unbounded homogeneous medium for example, then H_{M} is independent of r and Eq. (26) reduces to the expected expression for a time-invariant, space-invariant linear system:

$$\Phi(f,\beta) = \int_{-\infty}^{\infty} G(f,\nu)\, H_{M}(f,\nu) \int_{-\infty}^{\infty} e^{-j2\pi(\nu-\beta)\cdot\mathrm{r}}\, d\mathrm{r}\, d\nu\,. \tag{27a}$$

$$\Phi(f,\beta) = \int_{-\infty}^{\infty} G(f,\nu)\, H_{M}(f,\nu)\, \delta(\nu-\beta)\, d\nu\,, \tag{27b}$$

$$\Phi(f,\beta) = G(f,\beta)\, H_{M}(f,\beta)\,. \tag{27c}$$

b. The Transmitter

The transmitter array, the first block in Fig. 4, is characterized by a complex aperture function $A_T(f,\mathbf{r})$ ($\text{Amp}^{-1}\,\text{s}^{-1}$) relating the electrical input $x(t,\mathbf{r})$ (Amp) to the source distribution $g(t,\mathbf{r})$ (s^{-1}) through the expression [Ref. 5:p. 30]

$$G(f,\mathbf{r}) = X(f,\mathbf{r})\, A_T(f,\mathbf{r})\,. \tag{28}$$

The far-field directivity function $D_T(f,\boldsymbol{\nu})$ ($\text{m}^3\,\text{Amp}^{-1}\,\text{s}^{-1}$) is related to the complex aperture function through the transform [Ref. 5:p. 38]

$$D_T(f,\boldsymbol{\nu}) = \mathfrak{F}_{\mathbf{r}\text{-}\boldsymbol{\nu}}\{\, A_T(f,\mathbf{r})\,\}\,. \tag{29}$$

Using Eq. (29), the spatial Fourier transform of Eq. (28) is given by

$$G(f,\boldsymbol{\nu}) = X(f,\boldsymbol{\nu}) \overset{*}{_{\boldsymbol{\nu}}} D_T(f,\boldsymbol{\nu})\,, \tag{30a}$$

or

$$G(f,\boldsymbol{\nu}) = \int_{-\infty}^{\infty} X(f,\boldsymbol{\alpha})\, D_T(f,\boldsymbol{\nu}\text{-}\boldsymbol{\alpha})\, d\boldsymbol{\alpha}\,, \tag{30b}$$

where the symbol $\left(\overset{*}{_{\boldsymbol{\nu}}}\right)$ denotes a three-dimensional convolution with respect to $\boldsymbol{\nu}$. Equations (30a) and (30b) give the relationship between the electrical input and the source of the acoustic signal. The relationship between the input electrical signal and the velocity potential (the output of the medium block of Fig. 4) is obtained by

substituting Eq. (30b) into Eqs. (25) or (26). Let us introduce the simplifying assumption that the electrical input signal is independent of position, that is, $x(t,\mathbf{r}) = x(t)$ and $X(f,\boldsymbol{\nu}) = X(f)\,\delta(\boldsymbol{\nu})$. This is justified by the fact that the complex weights applied to the electrical signal (array shading and beam steering) are taken into account in $D_T(f,\boldsymbol{\nu})$, the far-field directivity function. With that assumption, Eq. (30a) becomes

$$G(f,\boldsymbol{\nu}) = X(f)\,\delta(\boldsymbol{\nu}) \overset{*}{_{\boldsymbol{\nu}}} D_T(f,\boldsymbol{\nu}), \tag{31a}$$

or

$$G(f,\boldsymbol{\nu}) = X(f)\,D_T(f,\boldsymbol{\nu}), \tag{31b}$$

which, when substituted into Eq. (25), gives the required relationship between the input electrical signal and the velocity potential at the output of the medium block,

$$\varphi(t,\mathbf{r}) = \int_{-\infty}^{\infty}\int_{-\infty}^{\infty} X(f)D_T(f,\boldsymbol{\nu})H_M(f,\boldsymbol{\nu};\mathbf{r})\,e^{j2\pi(ft-\boldsymbol{\nu}\cdot\mathbf{r})}\,d\boldsymbol{\nu}\,df. \tag{32}$$

A further restriction we impose to our problem is that the transmitter array is composed of point sources, has rectangular shape, is parallel to the XY plane, as shown in Fig. 3, and is centered at position $\mathbf{r}_s = (x_s, y_s, z_s)$. The array has dimensions $M_t \times N_t$ (first dimension along the X direction and second dimension

along Y), with interelement spacing d_{xt} meters along X and d_{yt} meters along the Y direction. Then, the far-field directivity function for M_t and N_t odd is given by [Ref. 5;ch. 4]

$$D_T(f,\nu) = \sum_{p=-\frac{M_t-1}{2}}^{\frac{M_t-1}{2}} \sum_{q=-\frac{N_t-1}{2}}^{\frac{N_t-1}{2}} c_{pq}(f)\, e^{j2\pi\nu\cdot \mathbf{r}_{pq}} , \qquad (33)$$

where $\mathbf{r}_{pq} = (pd_{xt} + x_s,\ qd_{yt} + y_s,\ z_s)$ represents the position of each element and $c_{pq}(f) = a_{pq}(f)\, e^{j\theta_{pq}(f)}$ is the complex weight associated with the element at position $\mathbf{r}_{pq}$.

c. The Receiver

The receiver array, the last block in Fig. 4, is characterized by a complex aperture function $A_R(f,\mathbf{r})$ (V s m^{-5}) relating the velocity potential $\varphi(t,\mathbf{r})$ to the electrical signal $y(t,\mathbf{r})$ (V m^{-3}) through the expression [Ref. 5:p. 31]

$$Y(f,\mathbf{r}) = \Phi(f,\mathbf{r})\, A_R(f,\mathbf{r}) . \qquad (34)$$

As stated earlier, we are not concerned with the signal processing done on the received signal. Our purpose is to predict the waveform at the output of each receiver array element. So, we consider the term $A_R(f,\mathbf{r})$ as pertaining to a single transducer element. The quantity $y(t,\mathbf{r})$ is the *electrical signal distribution* (V m^{-3}) due to the velocity potential $\varphi(t,\mathbf{r})$ at a point $\mathbf{r}$ on the transducer. In order

to obtain the total electrical signal $y(t)$ at the transducer terminals, we must integrate $y(t,\mathbf{r})$ over the whole transducer volume, that is, integrate with respect to $\mathbf{r}$,

$$Y(f) = \int_{-\infty}^{\infty} Y(f,\mathbf{r})\, d\mathbf{r}\,,$$

$$Y(f) = \int_{-\infty}^{\infty} \Phi(f,\mathbf{r})\, A_R(f,\mathbf{r})\, d\mathbf{r}\,. \tag{35}$$

For a point sensor located at $\mathbf{r}_r$, the complex aperture function is given by

$$A_R(f,\mathbf{r}) = A(f)\, \delta(\mathbf{r}-\mathbf{r}_r)\,, \tag{36}$$

which results in an electrical signal at the terminals given [see Eq. (35)] by

$$Y(f) = \Phi(f,\mathbf{r}_r)\, A(f)\,. \tag{37}$$

If the transducer is a pressure sensor, then $A(f)$ is proportional to the frequency f, that is, $A(f) \sim jf$ and $Y(f) \sim jf\Phi(f,\mathbf{r}_s) \sim$ pressure . For simplicity, we take $A(f)$ as unity, and a pressure sensor can be simulated by inserting a suitable filter into the block diagram of Fig. 4. So, the output electrical signal will be numerically equal to the velocity potential. The receiver array, like the transmitter, is a rectangular array of point sensors of dimension $M_r \times N_r$, parallel to the XY plane, with interelement spacings d_{xr} and d_{yr} meters, centered at $\mathbf{r}_r = (x_r, y_r, z_r)$. The

output electrical signal at each element (m,n), given by Eq. (37) with $A(f) = 1$ and $\mathbf{r}_r = \mathbf{r}_{mn} = (m\, d_{xr} + x_r\ ,\ n\, d_{yr} + y_r\ ,\ z_r)$, is

$$Y_{mn}(f) = \Phi(f,\mathbf{r}_{mn})\ , \tag{38}$$

or

$$y_{mn}(t) = \varphi(t,\mathbf{r}_{mn})\ . \tag{39}$$

d. Overall Transfer Function

The overall transfer function relates the output electrical signal $y_{mn}(t)$ at each point sensor (m,n) of the receiver array to the electrical input signal $x(t)$ at the transmitter array. Substituting Eq. (39) into Eq. (32) we obtain, for the output signal,

$$y_{mn}(t) = \int_{-\infty}^{\infty}\int_{-\infty}^{\infty} X(f)\ D_T(f,\nu)\ H_M(f,\nu;\mathbf{r}_{mn})\ e^{j2\pi(ft-\nu\cdot\mathbf{r}_{mn})}d\nu\ df, \tag{40a}$$

$$y_{mn}(t) = \int_{-\infty}^{\infty} X(f)\int_{-\infty}^{\infty} D_T(f,\nu)\ H_M(f,\nu;\mathbf{r}_{mn})\ e^{-j2\pi\nu\cdot\mathbf{r}_{mn}}\ d\nu\ e^{j2\pi ft}df. \tag{40b}$$

The last expression can be rewritten as

$$y_{mn}(t) = \int_{-\infty}^{\infty} X(f)\ H(f,\mathbf{r}_{mn})\ e^{j2\pi ft}df, \tag{40c}$$

or

$$y_{mn}(t) = \mathfrak{F}^{-1}_{t-f}\{\, X(f)\, H(f,\mathbf{r}_{mn})\,\}\,, \tag{40d}$$

where $H(f,\mathbf{r}_{mn})$ is the overall transfer function, given by

$$H(f,\mathbf{r}_{mn}) = \int_{-\infty}^{\infty} D_T(f,\boldsymbol{\nu})\, H_M(f,\boldsymbol{\nu};\mathbf{r}_{mn})\, e^{-j2\pi\boldsymbol{\nu}\cdot\mathbf{r}_{mn}}\, d\boldsymbol{\nu}\,. \tag{41}$$

Note that Eq. (40c) is valid only when the input electrical signal is independent of position and the receiver is a point sensor with unit frequency response, that is, $A(f) = 1$. On the other hand, Eq. (32) assumes only the independence of the input electrical signal with respect to position.

B. THE RANGE INDEPENDENT ACOUSTIC CHANNEL

In this section we will derive the expression for the overall transfer function for the particular case of a range independent medium. With reference to Fig. 3, the range independent medium characteristics change only with the Y (depth) direction, and the boundary conditions are independent of x and z; that is, the problem presents cylindrical symmetry.

1. Medium Transfer Function

In order to obtain the medium transfer function, we will solve the wave equation using a time-harmonic point source, that is,

$$\nabla^2\varphi(t,\mathbf{r}) - \frac{1}{c^2(y)}\frac{\partial^2}{\partial t^2}\varphi(t,\mathbf{r}) = e^{j2\pi f_o t}\,\delta(\mathbf{r}-\mathbf{r}_s)\,, \tag{42}$$

with suitable boundary conditions . The solution, as shown in Eq. (6d), is of the form $\varphi(t,\mathbf{r}) = \xi(\mathbf{r})\, e^{j2\pi f_o t}$ with $\xi(\mathbf{r})$ satisfying the Helmholtz wave equation

$$\nabla^2 \xi(\mathbf{r}) + k^2(y)\, \xi(\mathbf{r}) = \delta(\mathbf{r}-\mathbf{r}_s)\,, \tag{43}$$

where $k(y) = 2\pi f/c(y)$ is the depth dependent wave number. Applying the spatial Fourier transform with respect to x and z to Eq. (43), we obtain

$$k_y^2(y)\, \Xi(f_x,y,f_z) + \frac{d^2}{dy^2}\Xi(f_x,y,f_z) = e^{j2\pi(f_x x_s + f_z z_s)}\, \delta(y-y_s)\,. \tag{44}$$

where $k_y^2(y) = k^2(y) - 4\pi^2(f_x^2 + f_z^2)$ and $\Xi(f_x,y,f_z)$ is the spatial Fourier transform of $\xi(\mathbf{r})$ with respect to x and z. Solutions to Eq. (44) are usually obtained by approximate methods, most notably the WKB approximation. We can write the solution to Eq. (44), without loss of generality, as

$$\Xi(f_x,y,f_z) = \underbrace{a(y)\, \left\{ A\, e^{-j\theta_y(y)} + B\, e^{j\theta_y(y)} \right\}}_{\Psi}\, e^{j2\pi(f_x x_s + f_z z_s)}\,. \tag{45}$$

The (transformed) velocity potential, obtained from Eq. (45) and the assumed $\varphi(t,\mathbf{r}) = \xi(\mathbf{r})\, e^{j2\pi f_o t}$, is given by

$$\Phi(t,f_x,y,f_z) = \Xi(f_x,y,f_z)\, e^{j2\pi f_o t}\,. \tag{46}$$

The velocity potential $\varphi(t,\mathbf{r})$ is given by the inverse Fourier transform of Eq. (46) with respect to x and z, namely

$$\varphi(t,\mathbf{r}) = e^{j2\pi f_0 t}\int_{-\infty}^{\infty}\int_{-\infty}^{\infty}\Xi(f_x,y,f_z)\; e^{-j2\pi f_x x} e^{-j2\pi f_z z} df_x\; df_z\,. \tag{47}$$

Next, we will relate these results to those obtained in Section II-A-1c, the response of a linear time-invariant, space-variant system to a time-harmonic point source, as given by Eq. (6d), which can be written as

$$\varphi(t,\mathbf{r}) = e^{j2\pi f_0 t}\int_{-\infty}^{\infty} H(f_0,f_x,f_y,f_z;\mathbf{r})\; e^{-j2\pi f_x x_0} e^{-j2\pi f_y y_0} e^{-j2\pi f_z z_0} d\nu\,. \tag{48}$$

where $\mathbf{r}_0 = (x_0, y_0, z_0) = (x-x_s,\, y-y_s,\, z-z_s)$ and $d\nu = df_x\, df_y\, df_z$. In order to compare Eqs. (47) and (48), we rewrite Eq. (47) using the term Ψ defined in Eq. (45) as follows:

$$\varphi(t,\mathbf{r}) = e^{j2\pi f_0 t}\int_{-\infty}^{\infty}\int_{-\infty}^{\infty}\Psi\; e^{j2\pi(f_x x_s + f_z z_s)} e^{-j2\pi f_x x} e^{-j2\pi f_z z} df_x\; df_z\,. \tag{49a}$$

$$\varphi(t,\mathbf{r}) = e^{j2\pi f_0 t}\int_{-\infty}^{\infty}\int_{-\infty}^{\infty}\Psi\; e^{-j2\pi f_x x_0} e^{-j2\pi f_z z_0} df_x\; df_z\,. \tag{49b}$$

Comparing the Fourier transform expressions in Eqs. (48) and (49b), the term Ψ, obtained from the solution of the inhomogeneous wave equation when the source is a

unit amplitude, time-harmonic point source, is seen to be related to the medium transfer function through the transform

$$\Psi(f,f_x,y_o,f_z;y) = \mathfrak{F}^{-1}_{y_o\text{-}f_y}\{\, H_M(f,f_x,f_y,f_z;y)\,\}, \tag{50a}$$

or

$$\Psi(f,f_x,y_o,f_z;y) = \int_{-\infty}^{\infty} H_M(f,f_x,f_y,f_z;y)\; e^{-j2\pi f_y y_o} df_y\,, \tag{50b}$$

where y has been substituted for $\mathbf{r}$ as an argument of H_M in order to stress the depth-only dependence of the medium transfer function. Notice also that the arguments of Ψ have been written in accordance with the linear systems notation introduced in Section II-A-1.

The transfer function can then be obtained as the direct spatial Fourier transform of $\Psi(f,f_x,y_o,f_z;y)$ with respect to $y_o = y - y_s$. In the next section we will see that this last step is not necessary, so long as the transmitter array is composed of point sources.

2. **Output Electrical Signal**

The overall transfer function for a range independent medium can be computed from Eq. (41) by substitution of the expressions for $D_T(f,\boldsymbol{\nu})$ and the medium transfer function. As we just mentioned, it will not be necessary to compute the medium transfer function if the transmitter elements are point sources. The directivity function for the transmitter array is a sum of terms of the form $c_{pq}(f)\; e^{j2\pi\boldsymbol{\nu}\cdot\mathbf{r}_{pq}}$, where $\mathbf{r}_{pq} = (x_p\,,\, y_q\,,\, z_s)$ is the position of each transmitter

element. Substituting that general summation term into Eq. (41) and expanding the exponential factors yields the result that the overall transfer function is a summation—over p and q—of terms of the form

$$c_{pq}(f)\int_{-\infty}^{\infty} e^{j2\pi(f_x x_p+f_y y_q+f_z z_s)}\, H_M(f,f_x,f_y,f_z;y_n)\, e^{-j2\pi(f_x x_m+f_y y_n+f_z z_r)}\, d\nu\ ,$$

or

$$c_{pq}(f)\int_{-\infty}^{\infty} e^{-j2\pi f_x(x_m-x_p)}\, e^{-j2\pi f_y(y_n-y_q)}\, e^{-j2\pi f_z(z_r-z_s)}\, H_M(f,f_x,f_y,f_z;y_n)\, d\nu\ .$$

where $x_m = x_r+m\,d_{xr}$ and $y_n = y_r+n\,d_{yr}$ are the (x,y) coordinates of the receiver array elements, and the (x,y) coordinates of the transmitter array elements are $x_p = x_s+p\,d_{xt}$ and $y_q = y_s+q\,d_{yt}$. Recall from Section II-A-1 that the parameter r_o is the vectorial difference between observation point and source position. The integral in this last expression is the inverse spatial Fourier transform of the transfer function $H_M(f,f_x,f_y,f_z;y_n)$ with respect to f_x, f_y and f_z which yields a function of (x_o, y_o, z_o), where $x_o = x_m-x_p$, $y_o = y_n-y_q$, and $z_o = z_r-z_s$. But the transform with respect to f_y is already given by Eq. (50b) as the function $\Psi(f,f_x,y_o,f_z;y)$ obtained from the solution of the wave equation. As a result, we can rewrite the above last expression as

$$c_{pq}(f)\int_{-\infty}^{\infty}\int_{-\infty}^{\infty} \Psi(f,f_x,y_o,f_z;y)\, e^{-j2\pi f_x x_o}\, e^{-j2\pi f_z z_o}\, df_x\, df_z\ .$$

Therefore, the overall transfer function for the range-independent medium is given by

$$H(f,\mathbf{r}_{mn}) = \sum_{p=-\frac{N_t-1}{2}}^{\frac{N_t-1}{2}} \sum_{=-\frac{N_t-1}{2}}^{\frac{N_t-1}{2}} c_{pq}(f) \int_{-\infty}^{\infty}\int_{-\infty}^{\infty} \Psi(f,f_x,y_o,f_z;y_n)\, e^{-j2\pi f_x x_o} \times e^{-j2\pi f_z z_o}\, df_x\, df_z . \qquad (51)$$

The output electrical signal at each receiver position is given by Eq. (40c), repeated here for convenience:

$$y_{mn}(t) = \int_{-\infty}^{\infty} X(f)\, H(f,\mathbf{r}_{mn})\, e^{j2\pi f t} df, \qquad (40c)$$

where $H(f,\mathbf{r}_{mn})$ is given by Eq. (51). Again, we stress that Eq. (40c) incorporates three assumptions regarding the *linear* system:

- The input electrical signal is independent of position $\mathbf{r}$, that is, $x(t,\mathbf{r}) = x(t)$.
- The receiver array elements are point sensors, that is, $A_R(f,\mathbf{r}) = A(f)\,\delta(\mathbf{r}-\mathbf{r}_r)$.
- The sensors have unit frequency response, that is, $A(f) = 1$.

Equation (51) assumes, in addition:

- The transmitter array elements are point sources.
- The medium has range independent characteristics and boundary conditions.
- Transmitter array geometry is as described in Section I-A-2b.

a. An Alternative Representation

We will now compare our results, as given by Eqs. (51) and (40c), with the results obtained by solving the wave equation for a range-independent medium in cylindrical coordinates and written in terms of a Fourier-Bessel integral. DiNapoli and Deavenport [Ref. 4:p. 80], for example, use that representation as a starting point for the description of numerical methods applied to range independent problems.

The integral in Eq. (51) can be seen as the overall transfer function due to a single point source. From this point of view, $H(f,\mathbf{r}_{mn})$ is just the weighted sum of the transfer functions due to each transmitter array element, as one would expect for a parallel *connection* of linear systems. These elementary overall transfer functions $H_{pq}(f,\mathbf{r}_{mn})$ are given by

$$H_{pq}(f,\mathbf{r}_{mn}) = \int_{-\infty}^{\infty}\int_{-\infty}^{\infty} \Psi(f,f_x,y_o,f_z;y_n)\, e^{-j2\pi f_x x_o}\, e^{-j2\pi f_z z_o}\, df_x\, df_z \,. \tag{52}$$

The overall transfer function can then be written as

$$H(f,\mathbf{r}_{mn}) = \sum_{p=-\frac{M_t-1}{2}}^{\frac{M_t-1}{2}} \sum_{q=-\frac{N_t-1}{2}}^{\frac{N_t-1}{2}} c_{pq}(f)\, H_{pq}(f,\mathbf{r}_{mn}) \,. \tag{53}$$

Let us make a change of variables in the integral in Eq. (52), exploiting the fact that the dependence of $\Psi(f,f_x,y_o,f_z;y_n)$ with f_x and f_z occurs due to the factor $k_y^2(y) = k^2(y) - 4\pi^2(f_x^2 + f_z^2)$ in Eq. (44), that is, Ψ is a function of $(f_x^2 + f_z^2)$.

Introduce the variables f_r and γ such that

$$f_x = f_r \cos\gamma \quad \text{and} \quad f_z = f_r \sin\gamma\,, \tag{54}$$

which is a change from "rectangular" coordinates (f_x, f_z) to the "polar" coordinates (f_r, γ). With this change of variables, Eq. (52) becomes

$$H_{pq}(f, r_{mn}) = \int_0^{\infty} \Psi(f, f_r, y_o; y_n)\, f_r \int_0^{2\pi} e^{-j2\pi f_r (x_o \cos\gamma + z_o \sin\gamma)} d\gamma\, df_r\,, \tag{55}$$

where

$$\Psi(f, f_r, y_o; y_n) = \Psi(f, f_x, y_o, f_z; y_n)\Big|_{\substack{f_x = f_r \cos\gamma \\ f_z = f_r \sin\gamma}}. \tag{56}$$

Equation (55) can be written as

$$H_{pq}(f, r_{mn}) = \int_0^{\infty} \Psi(f, f_r, y_o; y_n)\, f_r \int_0^{2\pi} e^{-j2\pi f_r R_o \sin(\gamma+\alpha)} d\gamma\, df_r\,, \tag{57}$$

where $\sin\alpha = x_o / R_o$, $\cos\alpha = z_o / R_o$, and $R_o = \sqrt{x_o^2 + z_o^2}$. Because of the periodicity of the *sine* function, the term α can be dropped from the exponent without altering the result. The last integral can then be recognized as the zero-order Bessel function of the first kind [Ref. 6:p. 184], that is,

$$J_o(z) = \frac{1}{2\pi} \int_0^{2\pi} e^{-jz \sin \gamma} d\gamma , \tag{58}$$

which leads us to the Fourier-Bessel integral representation

$$H_{pq}(f, r_{mn}) = 2\pi \int_0^{\infty} \Psi(f, f_r, y_o; y_n)\, J_o(2\pi f_r R_o)\, f_r\, df_r . \tag{59}$$

Equation (59) is the same as Eq. (3.1) in [Ref. 4] if we perform the trivial change of variables $k_r = 2\pi f_r$. There, Ψ is interpreted as the depth dependent Green's function. Equation (59) is the starting point to several approaches to the range independent problem, both numerical and analytical [Ref. 4:pp. 80-134]. Using the Fourier-Bessel integral representation, the overall transfer function $H(f, r_{mn})$ can be written, from Eqs. (53) and (59), as

$$H(f, r_{mn}) = \sum_{p = -\frac{M_t - 1}{2}}^{\frac{M_t - 1}{2}} \sum_{q = -\frac{N_t - 1}{2}}^{\frac{N_t - 1}{2}} c_{pq}(f)\, 2\pi \int_0^{\infty} \Psi(f, f_r, y_o; y_n)\, J_o(2\pi f_r R_o)\, f_r\, df_r . \tag{60}$$

C. THE LAYERED WAVEGUIDE

In this section we will derive the function Ψ for the case of a three fluid medium waveguide, commonly referred to as the Pekeris waveguide.

1. Statement of The Problem

Figure 5 shows the relevant physical aspects for our derivation. The point source is at position (x_s, y_s, z_s) in medium II and the receiver is at (x, y, z) in the same medium. Medium II, with characteristic impedance $\rho_2 c_2$, is bounded at $y = 0$, the surface, by a fluid with characteristic impedance $\rho_1 c_1$ and at $y = D$, the bottom, by another fluid with characteristic impedance $\rho_3 c_3$. As described in Section B-1, in order to obtain Ψ, we need to solve the Helmholtz wave equation, Eq. (44), and isolate the terms with y dependence from the solution, as shown in Eq. (45). An inspection of those two expressions show us that by setting x_s and z_s to zero, the solution of the wave equation will be automatically the function Ψ. The wave equations that describe the propagation in the three media are:

$$k_{y1}^2 \Psi_1 + \frac{d^2}{dy^2} \Psi_1 = 0 , \tag{61}$$

$$k_{y2}^2 \Psi_2 + \frac{d^2}{dy^2} \Psi_2 = \delta(y-y_s) , \tag{62}$$

and

$$k_{y3}^2 \Psi_3 + \frac{d^2}{dy^2} \Psi_3 = 0 , \tag{63}$$

where $k_{yi}^2 = k_i^2 - 4\pi^2(f_x^2 + f_z^2)$, $k_i = 2\pi f / c_i$ and the subscripts 1, 2, and 3 refer to the three different media. The argument of Ψ has been dropped for simplicity. We seek the solution Ψ_2 because we shall be concerned only with those problems where both source and receiver are in medium II. The boundary conditions are the

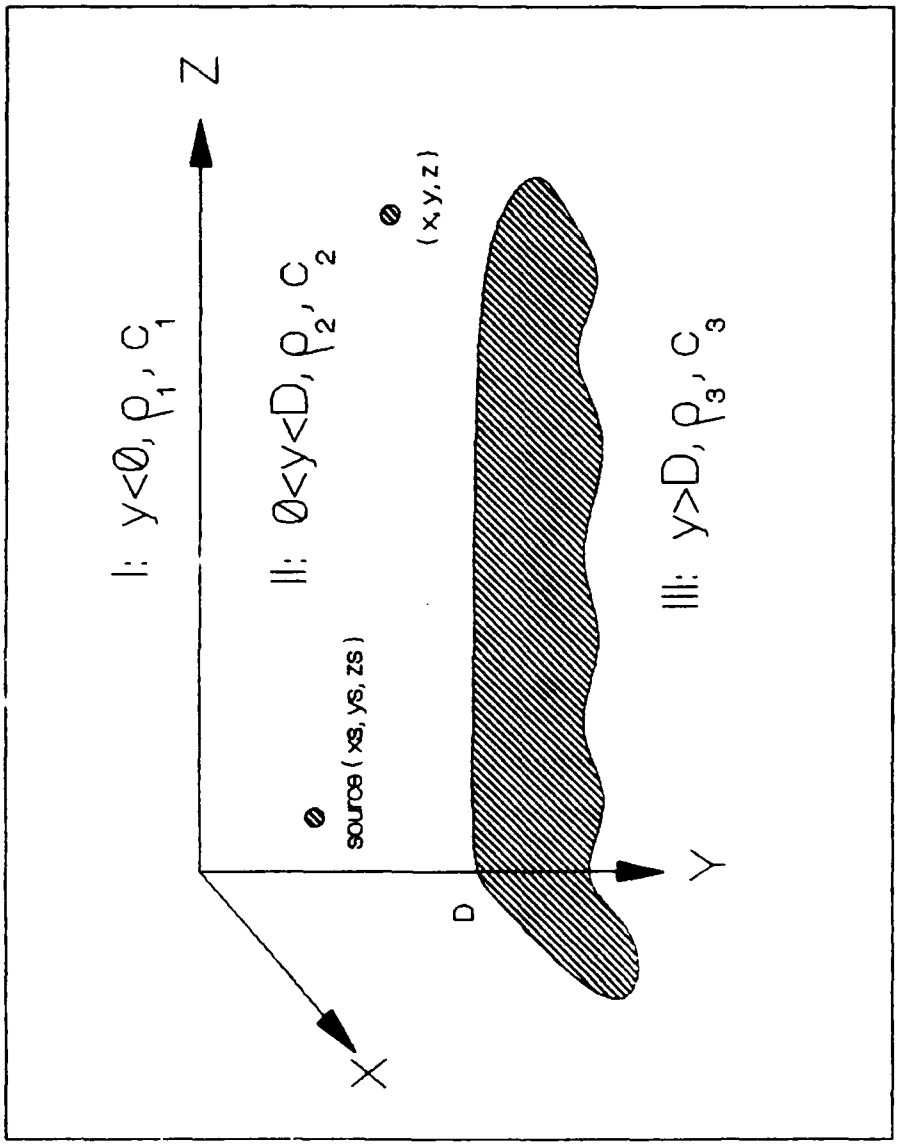

Fig. 5. The Three Layer Waveguide.

continuity of the acoustic pressure and the normal component of the acoustic particle velocity at each boundary. Acoustic pressure is related to the velocity potential by

$$P_i(f) = j2\pi f \rho_i \Psi_i , \tag{64}$$

and the normal component of the acoustic particle velocity at the boundaries is related to velocity potential by

$$U_{ni} = \frac{d}{dy} \Psi_i . \tag{65}$$

2. Solution

With the source located in medium II, the solutions in media I and III must be in the form of propagating waves moving outward from the boundaries. In media II, there are waves propagating in both directions—increasing and decreasing y—due to the reflections at the boundaries. The expected form of the solutions are

$$\Psi_1 = A_1 e^{jk_{y1} y} , \; y \le 0 , \tag{66}$$

$$\Psi_{2a} = A_{2a} e^{jk_{y2} y} + B_{2a} e^{-jk_{y2} y} , \; 0 \le y \le y_s , \tag{67}$$

$$\Psi_{2b} = A_{2b} e^{jk_{y2} y} + B_{2b} e^{-jk_{y2} y} , \; y_s \le y \le D , \tag{68}$$

and

$$\Psi_3 = B_3\, e^{-jk_{y3}\, y}\,,\; y \geq D\,. \tag{69}$$

The solution in medium II has been split in two in order to account for the point source, as usual in the Green's Function determination. Two more boundary conditions are necessary:

- Continuity of the solution Ψ_2 at $y = y_s$.
- Discontinuity of the first derivative of Ψ_2 at $y = y_s$.

The value of the discontinuity can be found by integrating Eq. (62) over a region $|\, y\text{-}y_s| < \epsilon$ and taking the limit as $\epsilon \to 0$. Performing this operation and taking into account that, in the limit, the integration of the continuous function Ψ_2 is zero, we obtain

$$\lim_{\epsilon \to 0} \int_{y_s-\epsilon}^{y_s+\epsilon} \frac{d^2}{dy^2}\, \Psi_2\, dy = 1\,, \tag{70a}$$

or

$$\frac{d}{dy}\, \Psi_{2b} \Big|_{y_s} - \frac{d}{dy}\, \Psi_{2a} \Big|_{y_s} = 1\,. \tag{70b}$$

a. Boundary Condition at $y = 0$

In order to obtain the expression that represents the continuity of pressure at $y = 0$, we equate the value of pressures due to Ψ_1 and Ψ_{2a}. Substituting the assumed solutions—Eqs. (66) and (67)—into Eq. (64) yields

$$\rho_1 A_1 = \rho_2 (A_{2a} + B_{2a}) . \tag{71}$$

For the normal component of particle velocity, Eq. (65) and the assumed solutions yield

$$k_{y1} A_1 = k_{y2} (A_{2a} - B_{2a}) . \tag{72}$$

Substituting Eq. (71) into (72), A_1 is eliminated and the relationship between the amplitudes of the solution Ψ_{2a} is found to be

$$\frac{B_{2a}}{A_{2a}} = R_{21} = \frac{\frac{\rho_1}{\rho_2} k_{y2} - k_{y1}}{\frac{\rho_1}{\rho_2} k_{y2} + k_{y1}} . \tag{73}$$

When k_{y2} is real, corresponding to propagating waves in medium II, the factor R_{21} is physically interpreted as the plane wave reflection coefficient at the surface.

b. Boundary Condition at $y = D$

Following the steps of the previous section, using the forms of the assumed solutions for Ψ_3 and Ψ_{2b} at $y = D$, we find

$$\rho_3 A_3 e^{-jk_{y3}D} = \rho_2 (A_{2b} e^{jk_{y2}D} + B_{2b} e^{-jk_{y2}D}), \quad (74)$$

and

$$-k_{y3} A_3 e^{-jk_{y3}D} = k_{y2} (A_{2b} e^{jk_{y2}D} - B_{2b} e^{-jk_{y2}D}). \quad (75)$$

Substituting Eq. (74) into (75), A_3 is eliminated and the relationship between the other two amplitude factors is found to be

$$\frac{A_{2b}}{B_{2b}} = R_{23} e^{-j2k_{y2}D} = \frac{\frac{\rho_3}{\rho_2} k_{y2} - k_{y3}}{\frac{\rho_3}{\rho_2} k_{y2} + k_{y3}} e^{-j2k_{y2}D}. \quad (76)$$

When k_{y2} is real, R_{23} has the physical meaning of the plane wave reflection coefficient at the bottom.

c. *Source Condition*

Using the results of the two last sections, Eqs. (73) and (76), the solutions in medium II become

$$\Psi_{2a} = A_{2a} (e^{jk_{y2}y} + R_{21} e^{-jk_{y2}y}), 0 \le y \le y_s. \quad (77)$$

and

$$\Psi_{2b} = B_{2b} (R_{23} e^{-j2k_{y2}D} e^{jk_{y2}y} + e^{-jk_{y2}y}), y_s \le y \le D. \quad (78)$$

The condition of continuity of Ψ_2 at $y = y_s$, applied to the above two equations, gives the relation between the amplitudes A_{2a} and B_{2b}:

$$\frac{A_{2a}}{B_{2b}} = \frac{R_{23}\ e^{-j\,2k_{y2}D}\ e^{jk_{y2}\,y_s} + e^{-jk_{y2}\,y_s}}{e^{jk_{y2}\,y_s} + R_{21}\,e^{-jk_{y2}\,y_s}}. \tag{79}$$

Finally, apply the condition on the derivative of Ψ_2 at $y = y_s$, as given by Eq. (70b), to obtain:

$$B_{2b}\,(R_{23}\,e^{-j\,2k_{y2}D}\,e^{jk_{y2}y_s} - e^{-jk_{y2}y_s}) - A_{2a}\,(e^{jk_{y2}y_s} - R_{21}\,e^{-jk_{y2}y_s}) = \frac{1}{jk_{y2}}, \tag{80}$$

which, together with Eq. (79), forms the necessary system of equations to obtain the two amplitude factors, B_{2b} and A_{2a}. Upon substitution of the expressions for B_{2b} and A_{2a} into Eqs. (77) and (78), we obtain the solutions Ψ_{2a} and Ψ_{2b}, which form the transformed transfer function $\Psi(f, f_x, y_o, f_z; y)$ we seek. Written in an abbreviated form, the final expression is

$$\Psi(f, f_x, y_o, f_z; y) = j\frac{1}{2k_{y2}}\,\frac{R_{23}\ e^{-j\,2k_{y2}D}\ e^{jk_{y2}\ y>} + e^{-jk_{y2}\ y>}}{1 - R_{21}\ R_{23}\ e^{-j\ 2k_{y2}D}}$$

$$\times\,(e^{jk_{y2}\ y<} + R_{21}\,e^{-jk_{y2}\ y<}), \tag{81}$$

where $0 \le y \le D$, $0 \le y_s \le D$, and, as usual, $y>$ is the greater and $y<$ the smaller between y and y_s.

3. Special Cases

In order to check the solution for the layered waveguide, we will now derive the expression for the output electrical signal in two special cases whose analytical solutions are known. These results will be used to check the computer implementation. In both cases, the input will be a time-harmonic point source.

a. Unbounded Homogeneous Medium (Free Space)

An unbounded homogeneous medium can be represented by Fig. 5 if the sound speeds c_i and densities ρ_i are equal for the three media. In this case, the reflection coefficients, as given by Eqs. (73) and (76), become zero. The transformed transfer function—Eq. (81)—reduces to

$$\Psi(f, f_x, y_o, f_z; y) = j\frac{1}{2k_{y2}}\, e^{-jk_{y2}y>}\, e^{jk_{y2}y<}, \tag{82a}$$

$$\Psi(f, f_x, y_o, f_z; y) = j\frac{1}{2k_{y2}}\, e^{-jk_{y2}(y> - y<)}, \tag{82b}$$

or

$$\Psi(f, f_x, y_o, f_z; y) = j\frac{1}{2k_{y2}}\, e^{-jk_{y2}|y - y_s|} = j\frac{1}{2k_{y2}}\, e^{-jk_{y2}|y_o|}. \tag{82c}$$

Note that the right hand side of Eq. (82c) is expressed in terms of y_o only, meaning that the unbounded homogeneous medium is space-invariant, as expected.

The overall transfer function $H(f,\mathbf{r})$ for the case of a point source is given by Eq. (51) with $M_t = N_t = c_{11}(f) = 1$. Substituting Eq. (82c) into Eq. (51) yields

$$H(f,\mathbf{r}) = \int_{-\infty}^{\infty}\int_{-\infty}^{\infty} j\frac{1}{2k_{y2}}\, e^{-jk_{y2}|y_o|}\, e^{-j2\pi f_x x_o}\, e^{-j2\pi f_z z_o}\, df_x\, df_z\,. \qquad (83)$$

The above integral is the expansion of a spherical wave into plane waves [Ref. 7:p. B-5] and the resultant overall transfer function is

$$H(f,\mathbf{r}) = -\frac{e^{-jk_2 R}}{4\pi R}, \qquad (84)$$

where $R = \| \mathbf{r}-\mathbf{r}_s \| = \sqrt{x_o^2 + y_o^2 + z_o^2} = \sqrt{(x-x_s)^2+(y-y_s)^2+(z-z_s)^2}$.

The output electrical signal $y(t)$—or velocity potential $\varphi(t,\mathbf{r})$, in our case—is given by Eq. (40c). Substituting Eq. (84) and $X(f) = \delta(f-f_o)$—for the time-harmonic source—into Eq. (40c) yields

$$y(t) = -\frac{1}{4\pi R}\, e^{j(2\pi f_o t - k_o R)}, \qquad (85)$$

where $k_o = 2\pi f_o / c_2$. Equation (85) is just the expression for a spherical wave, since R is the distance between source and receiver.

b. Surface Reflection

Consider the case where media II and III are the same, that is, $c_2 = c_3$ and $\rho_2 = \rho_3$. As a result, R_{23} is zero and Ψ reduces to

$$\Psi(f,f_x,y_o,f_z;y) = j\frac{1}{2k_{y2}}\, e^{-jk_{y2}y_>}\,(e^{jk_{y2}y_<} + R_{21}\, e^{-jk_{y2}y_<}), \qquad (86a)$$

$$\Psi(f,f_x,y_o,f_z;y) = j\frac{1}{2k_{y2}}\left(e^{-jk_{y2}(y> - y<)} + R_{21}\, e^{-jk_{y2}(y> + y<)}\right), \qquad (86b)$$

or

$$\Psi(f,f_x,y_o,f_z;y) = j\frac{1}{2k_{y2}}\left(e^{-jk_{y2}|y - y_s|} + R_{21}\, e^{-jk_{y2}|y + y_s|}\right), 0 \le y,\ 0 \le y_s\,. \qquad (86c)$$

Comparing Eqs. (82c) and (86c), we see that this problem can be treated by considering a homogeneous medium with two point sources, one located at y_s with unit strength, and the second located at $-y_s$ with strength R_{21}. The output electrical signal due to the first term in Eq. (86c) has already been computed in the previous section, and is given by Eq. (85). In the second term, we have the factor R_{21}, also a function of f_x and f_z through the dependence on k_{y1} and k_{y2}. When performing the inverse spatial Fourier transform to obtain $H(f,r)$, it would be easier if R_{21} were constant. If we consider the boundary I-II as pressure release , that is, $\rho_1/\rho_2 = 0$, then, by Eq. (73), $R_{21} = -1$. In this case, Eq. (86c) reduces to

$$\Psi(f,f_x,y_o,f_z;y) = j\frac{1}{2k_{y2}}\left(e^{-jk_{y2}|y_o|} - e^{-jk_{y2}|y_o'|}\right). \qquad (87)$$

where $y_o' = y-(-y_s)$. From the results in the previous section, the output electrical signal is, by superposition,

$$y(t) = -\frac{1}{4\pi R}\, e^{j(2\pi f_o t - k_o R)} + \frac{1}{4\pi R'}\, e^{j(2\pi f_o t - k_o R')}, \qquad (88)$$

where $R' = \| \mathbf{r}-\mathbf{r}'_s \| = \sqrt{x_o^2 + y_o'^2 + z_o^2} = \sqrt{(x-x_s)^2+(y+y_s)^2+(z-z_s)^2}$. If the distance R is large compared to the depth of the source y_s, a simplification is possible. From Fig. 6, for large R , $R \approx R_s - \Delta R$, $R' \approx R_s + \Delta R$ and $\Delta R \approx y_s \sin\theta = y_s\, y_r / R_s$, where R_s is the distance from the receiver to the midpoint between the source and its image. With these approximations and letting $R \approx R' \approx R_s$ in the amplitude factor, Eq. (88) becomes [Ref. 7:pp. 170, 408]

$$y(t) = -j\frac{1}{2\pi R_s}\, e^{j(2\pi f_o t - k_o R_s)}\, \sin\left(\frac{k_o\, y_s\, y_r}{R_s}\right) . \tag{89}$$

D. SUMMARY

The transformed transfer function $\Psi(f, f_x, y_o, f_z; y)$ for a range-independent medium is the solution to the inhomogeneous Helmholtz wave equation

$$k_y^2(y)\, \Psi + \frac{d^2}{dy^2}\, \Psi = \delta(y-y_s) , \tag{90}$$

with suitable boundary conditions, where $k_y^2 = k^2 - 4\pi^2(f_x^2 + f_z^2)$ and $k = 2\pi f / c$.

Under the conditions stated in Section II-B-2, related to Eq. (51), the overall transfer function for a range-independent medium is given by

$$H(f, \mathbf{r}_{mn}) = \sum_{p\,=\,-\frac{M_t-1}{2}}^{\frac{M_t-1}{2}} \sum_{q\,=\,-\frac{N_t-1}{2}}^{\frac{N_t-1}{2}} c_{pq}(f) \int_{-\infty}^{\infty}\int_{-\infty}^{\infty} \Psi(f, f_x, y_o, f_z; y_n)\, e^{-j2\pi f_x x_o} \times e^{-j2\pi f_z z_o}\, df_x\, df_z , \tag{51}$$

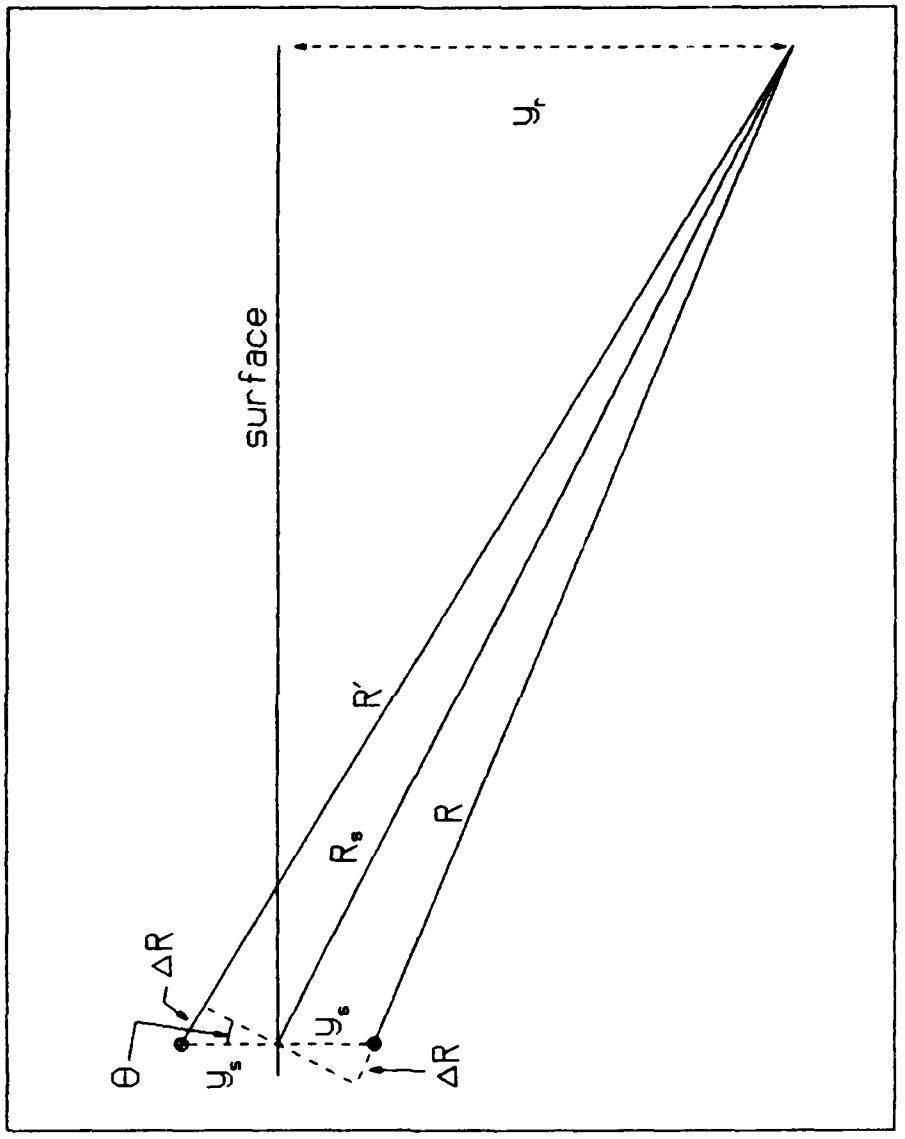

Fig. 6. Geometry of Surface Reflection.

where the transmitter array is rectangular, centered at (x_s, y_s, z_s), parallel to the XY plane, with odd dimensions $M_t \times N_t$, complex weights $c_{pq}(f)$, and with elements positioned at $x_p = x_s + px$, $y_q = y_s + qy$, and $z = z_s$. Also, $x_o = x_m - x_p$, $y_o = y_n - y_q$, and $z_o = z_r - z_s$. The overall transfer function $H(f, \mathbf{r}_{mn})$ can also be expressed as

$$H(f,\mathbf{r}_{mn}) = 2\pi \sum_{p=-\frac{M_t-1}{2}}^{\frac{M_t-1}{2}} \sum_{q=-\frac{N_t-1}{2}}^{\frac{N_t-1}{2}} c_{pq}(f) \int_0^\infty \Psi(f, f_r, y_o; y_n) \times J_o(2\pi f_r R_o)\, f_r\, df_r , \qquad (60)$$

where $f_r = \sqrt{f_x^2 + f_z^2}$, $R_o = \sqrt{x_o^2 + z_o^2}$, and

$$\Psi(f, f_r, y_o; y_n) = \Psi(f, f_x, y_o, f_z; y_n)\Big|_{\substack{f_x = f_r \cos\gamma \\ f_z = f_r \sin\gamma}} . \qquad (56)$$

The output electrical signal $y_{mn}(t)$, under the same conditions stated for the overall transfer function, is given by

$$y_{mn}(t) = \int_{-\infty}^{\infty} X(f)\, H(f, \mathbf{r}_{mn})\, e^{j2\pi f t} df , \qquad (40c)$$

where $H(f, \mathbf{r}_{mn})$ is given by Eqs. (51) or (60).

The layered waveguide illustrated in Fig. 5 is characterized by the transformed medium transfer function

$$\Psi(f,f_x,y_o,f_z;y) = j\frac{1}{2k_{y2}}\frac{R_{23}\ e^{-j\,2k_{y\,2}\,D}\ e^{jk_{y2}\ y>}\ +\ e^{-jk_{y2}\ y>}}{1\ -\ \ R_{2\,1}\ R_{2\,3}\ e^{-j\ 2k_{y2}D}}$$

$$\times\ (e^{jk_{y2}\ y<}\ +\ R_{21}\ e^{-jk_{y2}\ y<}\ )\ , \qquad (81)$$

which is valid for $0 \le y \le D$, $0 \le y_s \le D$, and where R_{21} is given by Eq. (73) and R_{23} by Eq. (76). If all three media have the same acoustic characteristics, then Eq. (81) reduces to

$$\Psi(f,f_x,y_o,f_z;y) = j\frac{1}{2k_{y2}}\ e^{-jk_{y2}|y_o|}\ , \qquad (82c)$$

and the corresponding output electrical signal is given by

$$y(t) = -\frac{1}{4\pi R}\ e^{j(2\pi f_o t\ -\ k_o R)}\ , \qquad (85)$$

where R is the distance from source to receiver. In the case where media II and III are the same and the surface is pressure release, the function Ψ is given by

$$\Psi(f,f_x,y_o,f_z;y) = j\frac{1}{2k_{y2}}\ (e^{-jk_{y2}|y_o|}\ -e^{-jk_{y2}|y_o'|})\ , \qquad (87)$$

where $y_o' = y + y_s$. The output electrical signal, when the source-receiver distance is large compared to the source depth, is given by

$$y(t) = -j\frac{1}{2\pi R_s} e^{j(2\pi f_o t - k_o R_s)} \sin\left(\frac{k_o\, y_s\, y_r}{R_s}\right), \tag{89}$$

where R_s is the distance from the receiver to the midpoint between the source and its surface image.

III. IMPLEMENTATION AND RESULTS

In this chapter, a computer implementation of the range independent medium equations is described. Although only the medium transfer function of the layered waveguide is implemented, the modular nature of the linear systems approach enables us to analyze the results and draw conclusions valid for the more general case. Equation (60) illustrates this point. The summations and the coefficients $c_{pq}(f)$ in that equation represent the transmitter array. The Bessel function $J_o(2\pi f_r R_o)$ is the range dependent factor. The function $\Psi(f, f_x, y_o, f_z; y)$—from now on referred to as the medium transfer function, for simplicity—is the (range independent) medium dependent factor.

Our purpose is to have a working algorithm to test the results from the previous chapter. Care has been taken to enable the implementation of other medium transfer functions, allowing for depth dependent speed of sound, so that the program can be used as an academic tool. Speed and style were secondary objectives.

The implementation is based on Eq. (60), the Fourier-Bessel integral representation.

A. IMPLEMENTED EQUATIONS

1. Medium Transfer Function

The medium transfer function $\Psi(f, f_r, y_o; y)$ is an oscillatory or exponential function of k_{y2}—as seen in Eq. (81)—which, in turn, is a function of $(f_x^2 + f_z^2) = f_r^2$. The function Ψ is easier analyzed in terms of k_{y2} than in terms of $f_r =$

$= \sqrt{(f/c_2)^2 - (k_{y2}/2\pi)^2}$, which is nonlinear. Therefore, Ψ will be treated as a function of k_{y2}, and the integral term in the expression for the overall transfer function, Eq. (60), will be modified accordingly.

a. Ψ as a Function of k_{y2}

The function Ψ is already expressed in terms of k_{y2} in Eq. (81). The reflection coefficients, on the other hand, are expressed in terms of k_{y1}, k_{y2}, and k_{y3}. In this section we establish the relationships between k_{y2} and the quantities f_r, k_{y1}, and k_{y3}. These relationships will enable us to represent the reflection coefficients in terms of the variable k_{y2}, as well as to change the variable of integration in the expression for the overall transfer function to k_{y2}.

The correspondence between k_{y2} and f_r is one-to-one. When $f_r \leq (f/c_2)$, k_{y2} is taken as the positive root $2\pi\sqrt{(f/c_2)^2 - f_r^2}$, a consequence of our choice of solutions, Eqs. (67) and (68). When $f_r > (f/c_2)$, k_{y2} is imaginary, corresponding to an exponentially decaying Ψ. When all factors in Eq. (81) are multiplied out, Ψ is seen to be composed of a sum of factors of the form

$$A\, e^{-jk_{y2}\alpha},$$

where α is a nonnegative real number. In order to have Ψ be a decreasing exponential, the negative root must be chosen when k_{y2} is imaginary. Similar reasoning yields the same results regarding k_{y1} and k_{y3}, which can be summarized as follows:

$$k_{yi} = \begin{cases} +\sqrt{k_i^2 - k_r^2} \;, & k_r < k_i \\ \\ -j\sqrt{k_r^2 - k_i^2} \;, & k_r > k_i \end{cases} \;, \tag{91}$$

where $i = 1$, 2 or 3 , $k_r = 2\pi f_r$ and $k_i = 2\pi f / c_i$. Using Eq. (91), the wavenumber y-components k_{y1} and k_{y3} can be expressed in terms of k_{y2} as

$$k_{yp} = \begin{cases} +\sqrt{k_p^2 - k_2^2 + k_{y2}^2} \;, & k_r < k_p \\ \\ -j\sqrt{k_2^2 - k_{y2}^2 - k_p^2} \;, & k_r > k_p \end{cases} \;, \tag{92}$$

where $p = 1$ or 3, and $k_r = \sqrt{k_2^2 - k_{y2}^2}$. Using Eq. (91), the integrations over f_r can be transformed into integrations over k_{y2}. Using Eq. (92), the reflection coefficients R_{21} and R_{23} , as given by Eqs. (73) and (76), can be expressed in terms of k_{y2}.

b. Air, Water, Fast Bottom Waveguide

The present implementation of the medium transfer function assumes that $c_1 < c_2$. When the surface is almost pressure release, which is the case of the air-water interface, and the bottom is fast, $c_3 > c_2$, the medium transfer function is composed of many sharp peaks, which presents some difficulties for integration routines.

(1) Poles of the Medium Transfer Function. When the surface is pressure release, that is, $R_{21} = -1$, Eq. (81) reduces to

$$\Psi(f,k_{y2},y_o;y) = -\frac{1}{k_{y2}} \frac{R_{23}\ e^{-j\,2k_{y\,2}\,D}\ e^{jk_{y2}y>} + \ e^{-jk_{y2}y>}}{1 + \ R_{2\,3}\ e^{-j\,2\,k_{y\,2}D}} \sin(\ k_{y2}\ y<)\ , \quad (93)$$

which is valid for $0 \le y \le D$ and $0 \le y_s \le D$. If the bottom is fast, $k_2 > k_3$, and, from Eq. (91), there is a range of values of k_r for which k_{y2} is real while k_{y3} is imaginary, that is, $k_3 < k_r < k_2$ or $0 < k_{y2} < \sqrt{k_2^2 - k_3^2}$. For this range of values of k_{y2}, the reflection coefficient R_{23}, given by

$$R_{23} = \frac{\frac{\rho_3}{\rho_2}\ k_{y2} - k_{y3}}{\frac{\rho_3}{\rho_2}\ k_{y2} + k_{y3}}, \quad (94)$$

becomes a unit magnitude complex number,

$$R_{23} = e^{j\,2\phi}\ , \quad (95)$$

where

$$tan\ \phi = -\frac{\rho_2}{\rho_3}\frac{Im\{\ k_{y3}\ \}}{k_{y2}} = \frac{\rho_2}{\rho_3}\frac{\sqrt{k_2^2 - \ k_{y2}^2 - k_3^2}}{k_{y2}}. \quad (96)$$

In this case, the denominator of the expression for Ψ, Eq. (93), may have zeros, given by

$$1 + R_{23}\ e^{-j\,2k_{y2}D} = 0\ , \quad (97a)$$

$$1 + e^{-j2(k_{y2}D - \phi)} = 0 . \tag{97b}$$

Therefore,

$$\phi - k_{y2}D = (2n + 1)\frac{\pi}{2}, \quad n = 0, 1, 2,... \tag{98a}$$

or

$$tan\ k_{y2}D = \frac{-1}{tan\ \phi} = -\frac{\rho_3}{\rho_2}\frac{k_{y2}}{\sqrt{k_2^2 - k_{y2}^2 - k_3^2}}, \tag{98b}$$

which can be expressed as

$$tan\ \theta = -\frac{\rho_3}{\rho_2}\frac{\theta}{\sqrt{a^2 - \theta^2}}, \tag{99}$$

where $\theta = k_{y2}D$ and $a = D\sqrt{k_2^2 - k_3^2}$. Solutions to the above transcendental equation in terms of $k_{y2} = \theta/D$ are the poles of the medium transfer function, for the case of a pressure release surface, Eq. (93), and a fast bottom. The physical interpretation of these poles is that they represent the discrete *eigenvalues* k_{y2n} corresponding to the *trapped* or *normal modes* in the waveguide[Ref. 8:pp. 430-440]. The graphical solution of Eq. (99) [Ref. 8:p. 438] reveals that:

- Poles exist only if $a > \pi/2$. If $a \gg \pi$, the poles will be separated by $\Delta k_{y2} \approx \pi/D$.
- The total number of poles is given by the integer number equal to $[(a/\pi) - 0.5]$ or, if the result is not integer, its nearest larger integer.

When the surface is almost pressure release, that is, $R_{21} \approx -1$, the medium transfer function presents peaks at values of k_{y2} corresponding to the poles computed as above.

2. Overall Transfer Function

In order to change the variable of integration in Eq. (60), the interval of integration $f_r \in (0, \infty)$ is subdivided into $(0, f/c_2)$ and $(f/c_2, \infty)$. After the change of variables according to Eq. (91) and a rearrangement, Eq. (60) becomes

$$H(f, r_{mn}) = \int_{\Gamma} \frac{1}{2\pi} \sum_p \sum_q c_{pq}(f)\, \Psi(f, k_{y2}, y_o; y_n)\, J_o(k_r R_o)\, k_{y2}\, dk_{y2}\,, \qquad (100)$$

where the path of integration Γ consists of the imaginary axis over the interval $(-j\infty, j0)$ plus the interval $(0, f/c)$ on the real axis. The summations over p and q are as indicated in Eq. (60).

B. THE SUBROUTINES

In this section we describe the subroutines and present the results for some examples. Also, a description of the main program and some auxiliary subroutines is given, which will help to clarify some aspects of the implementation[1].

---

[1]The main program and auxiliary routines were written by Dr. Lawrence J. Ziomek, at the Naval Postgraduate School, as part of an ongoing research project in model-based signal processing.

1. Main Program and Auxiliary Routines

The main program's simplified pseudo-code is shown in Fig. 7. It consists basically of calls to subroutines. The *readin* subroutine reads the input data, consisting of transmitted signal characteristics, transmitter and receiver array data, medium characteristics, and control data, including the *ocean medium transfer function* (OCNTF) variable used to select a transfer function, when more than one type of transfer function is implemented. The *ccq* subroutine generates the input electrical signal $x(t)$. The *chfmn* subroutine computes the overall transfer function, Eq. (100), and its estimated error. The *phfmn* subroutine provides a tabular output for the values of the overall transfer function and its error. The *calyce* subroutine computes the output electrical signal, according to Eq. (40c).

```
Main Program   /computes output waveform of an acoustic channel/
EXECUTE Readin   /read input data/
    EXECUTE Ccq   /generate input electrical signal/
    EXECUTE Chfmn   /compute overall transfer function/
    IF (flag print is TRUE) THEN
        EXECUTE Phfmn   /print overall transfer function/
    END IF
    EXECUTE Calyce   /compute output electrical signal/
End Main Program
```

Fig. 7. Simplified Pseudo-Code of the Main Program.

a. Subroutine Ccq

The subroutine *ccq* generates the input electrical signal $x(t)$, using the complex envelope representation. From the specifications read as input data, this subroutine computes the time samples of a reference complex envelope and its Fourier series coefficients. The Fourier series is truncated, yielding the complex envelope of the transmitted signal.

(1) Complex Signal Representation. An amplitude and angle modulated carrier $r(t)$ can be represented by its complex envelope $\tilde{r}(t)$ as [Ref. 5:pp. 177, 182]

$$r(t) = Re\{\ \tilde{r}(t)\ e^{j2\pi f_c t}\ \}\ , \tag{101}$$

where

$$\tilde{r}(t) = a(t)\ e^{j\theta(t)}\ , \tag{102}$$

$a(t)$ is the (real) amplitude modulating signal (Amp), $\theta(t)$ is the angle modulating signal (rad), and f_c is the carrier frequency (Hz). The Fourier transform of the signal is related to its complex envelope transform by [Ref 5:p. 187]

$$R(f) = 0.5[\tilde{R}(f - f_c) + \tilde{R}^*(-f - f_c)]\ . \tag{103}$$

For a rectangular-envelope LFM pulse, $a(t)$ and $\theta(t)$ are given by

$$a(t) = \begin{cases} A\ , |t| \leq T_P/2 \\ 0\ , |t| > T_P/2 \end{cases}\ , \tag{104}$$

and

$$\theta(t) = \frac{\pi \ Sw}{T_P} t^2 = D_P \ t^2, \tag{105}$$

where A is the (constant) amplitude (Amp), T_P is the pulse length (s), Sw is the swept bandwidth (Hz) and D_P is the phase-deviation constant (rad s^{-2}). Both Sw and D_P are allowed to be either positive or negative, corresponding to the ***up chirp*** and *down chirp* LFM pulses, respectively. If the modulated signal $r(t)$ is made periodic with period T_o, then the complex envelope can be represented by the Fourier series

$$\tilde{r}(t) = \sum_{k = -K}^{K} b_k \ e^{j 2\pi k f_o t}, \tag{106}$$

where

$$b_k = \frac{1}{T_o} \int_{-T_o/2}^{T_o/2} \tilde{r}(t) \ e^{-j 2\pi k f_o t} \ dt. \tag{107}$$

and $f_o = 1/T_o$. Equation (106) assumes a complex envelope bandlimited to Kf_o. From Equation (106), the transform of the complex envelope is given by

$$\tilde{R}(f) = \sum_{k = -K}^{K} b_k \ \delta(f - kf_o). \tag{108}$$

If the complex envelope is sampled with sampling period $T_s = T_o/(2K+1)$, which is basically the Nyquist rate, then, from Eqs. (106) and (107),

$$\tilde{r}(lT_s) = \sum_{k=-K}^{K} b_k \, e^{j2\pi kl/L}, \tag{109}$$

and

$$b_k = \frac{1}{L} \sum_{l=-K}^{K} \tilde{r}(lT_s) \, e^{-j2\pi kl/L}, \tag{110}$$

where $T_s = T_o/L$ is the sampling period, and $L = 2K+1$ is the total (odd) number of time and frequency samples. From Eqs. (103) and (108), the signal transform is given by

$$R(f) = 0.5 \sum_{k=-K}^{K} \{ b_k \, \delta(f - f_c - kf_o) + b_k^* \, \delta(-f - f_c - kf_o) \}, \tag{111}$$

from which the sampled signal can be derived as

$$r(lT_s) = Re \left\{ \sum_{k=-K}^{K} b_k \, e^{j2\pi kl/L} \, e^{j2\pi f_c lT_s} \right\} \tag{112}$$

(2) Subroutine Description. Figure 8 lists the pseudo-code of the subroutine *ccq*. The main input data for the subroutine are:

- Pulse length T_P, and pulse period (or pulse repetition period) T_o.
- Swept bandwidth S_W and pulse amplitude A.
- Maximum order of frequency component to be processed, K_{max}. The number of frequency components to be processed is $(2\,K_{max} + 1)$.
- Sampling rate multiplier S_R, a term to be multiplied by the Nyquist rate in order to obtain the actual sampling rate.
- Carrier frequency f_c .
- A flag *test* used to indicate option for plotting.

```
Subroutine Ccq

    Compute data for reference signal:

        total number of samples L for the complex envelope  /Eq. (114)/

        sample period TS for the complex envelope  /Eq. (113)/

        phase-deviation constant DP  /Eq. (105)/

    Generate samples of ref. signal complex envelope  /Eq. (102)/

    Compute complex Fourier coefficients  /Eq. (110)/

    IF (flag test is TRUE) THEN

        Compute and plot transmitted signal  /Eq. (116)/

    END IF

End Subroutine Ccq
```

Fig. 8. Simplified Pseudo-Code for the Signal Generator Subroutine.

The total number of samples for the complex envelope is given by

$$L = T_o / T_s \,, \tag{113}$$

where T_o and T_s are the pulse repetition period and complex envelope sampling period, respectively. The sampling frequency $f_s = 1/T_s$ is the product of the sampling rate multiplier S_R by the Nyquist rate, twice the complex envelope bandwidth. In terms of the input parameters listed earlier, Eq. (113) can be rewritten as

$$L \approx T_o \overbrace{S_R \; 2 \; (\underbrace{|S_W|}_{\approx BW(\text{envelope})} + 2/T_P)}^{f_s} \,, \tag{114}$$

which is the expression used in the subroutine. If the number of samples is less than the number of frequency components to be processed, $(2\,K_{max} + 1)$, L is increased accordingly. If the computed value of L is even, the result is increased by one. The phase-deviation constant D_P and the sampling period T_S are computed according to Eqs. (105) and (113), respectively.

The subroutine proceeds to compute the samples of the complex envelope of the reference signal—using Eqs. (102), (104) and (105)—at the time instants $t = l\,T_S$. The Fourier coefficients are computed next, using Eq. (110).

The signal to be transmitted is defined by multiplying the Fourier coefficient series $\{b_k\}$—computed for the reference signal—by a *window* of length

$(2\,K_{max} + 1)$. The simple truncation, which corresponds to a rectangular window, is avoided because of the ringing it would cause on the waveform. Instead, the Hamming window

$$w(n) = 0.54 + 0.46\ cos(\pi\ n/K_{max})\ ,\ \ -K_{max} \leq n \leq K_{max}\ , \tag{115}$$

is used. Therefore, the transmitted signal and its complex envelope are given by

$$x(lT_s) = Re\left\{ \sum_{k\ =\ -K_{max}}^{K_{max}} w(k)\ b_k\ e^{j2\pi kl/L}\ e^{j2\pi f_c lT_s} \right\},\ -K \leq l \leq K\ , \tag{116}$$

and

$$\tilde{x}(lT_s) = \sum_{k\ =\ -K_{max}}^{K_{max}} w(k)\ b_k\ e^{j2\pi kl/L}\ ,\ -K \leq l \leq K\ , \tag{117}$$

The transform of the transmitted signal is given, from Eq. (116), by

$$X(f) = 0.5 \sum_{k\ =\ -K_{max}}^{K_{max}} w(k)\ \{\ b_k\ \delta(f - f_c - kf_0) + b_k^*\ \delta(-f - f_c - kf_0)\ \}\ . \tag{118}$$

While the sampling rate is high enough for the complex envelope representation, the signal $x(t)$ usually requires a higher rate. In order to recover the signal from the Fourier coefficients, the series $\{b_k\}$ must be padded with zeros, so that the modulated signal samples occur more than twice per carrier period. Both

the subroutines *ccq* and *calyce*, to be described next, use six samples per carrier period for plotting purposes, for a total of $6f_cT_o$ samples on the interval $(-T_o/2\ ,\ T_o/2)$. This zero padding is accomplished by using the value $L_c = 6f_cT_o$ instead of L in Eq. (116).

b. Subroutine Calyce

The subroutine *calyce* computes the output electrical signal, both in complex envelope $\tilde{y}(t)$ and in band limited $y(t)$ forms.

(1) Sampled Output Signal. The electrical signal $y_{mn}(t)$ at the output of the element (m,n) in the receiver array is given by Eq. (40c). Substitution of the expression for the input signal transform, Eq. (118), into Eq. (40c) yields

$$y_{mn}(lT_s) = Re\left\{ \sum_{k\,=\,-I_{max}}^{I_{max}} w(k)\, b_k\, H(f_c + kf_o, \mathbf{r}_{mn})\, e^{j2\pi kl/L}\, e^{-j2\pi f_c lT_s} \right\}, \quad (119)$$

after performing the integration indicated in Eq. (40c), and where $f_oT_s = 1/L$. From the definition of the complex envelope, Eq. (101), the sampled complex envelope of the output signal is given, by inspection of Eq. (119), by

$$\tilde{y}_{mn}(lT_s) = \sum_{k\,=\,-I_{max}}^{I_{max}} w(k)\, b_k\, H(f_c + kf_o, \mathbf{r}_{mn})\, e^{j2\pi kl/L}\,. \quad (120)$$

Equations (119) and (120) are both implemented in the subroutine *calyce* The observations made about the recovery of the signal from its Fourier coefficients—regarding the zero padding of Fourier coefficients—are also valid for $y(t)$. In order

to have a correct reconstruction of $y(t)$, the constant L in Eq. (119) is substituted by $L_c = 6f_c T_o$, corresponding to six samples per carrier period.

(2) Subroutine Description. Figure 9 lists the pseudo-code of the subroutine *calyce*. The main input data for this subroutine, besides those listed for the subroutine *ccq*, are a three-dimensional array with the values of the overall transfer function for each frequency $(f_c + kf_o)$ and position (m,n) in the receiver array, and the Fourier coefficients b_k computed in the subroutine *ccq*.

The computation of the total number of samples L and sampling period T_s are as described in the previous section, in connection to the generation of the transmitted signal. The complex envelope samples $\tilde{y}_{mn}(lT_s)$ are computed according to Eq. (120). The signal samples $y_{mn}(lT_s)$ are computed using Eq. (119), with zero padding.

```
Subroutine Calyce
    Compute:
        total number of samples L for the complex envelope
        sample period TS for the complex envelope
    Compute complex envelope samples   /Eq. (120)/
    Compute and plot signal   /Eq. (119)/
End Subroutine Calyce
```

Fig. 9. Simplified Pseudo-Code for the Subroutine *Calyce*.

2. Computing the Overall Transfer Function

The computation of the overall transfer function is performed by a group of subprograms subordinated to the subroutine *chfmn*, called by the main program. The relationships between the subroutines used for this implementation are shown in Fig. 10. The program was implemented in FORTRAN, with most of the variables shared through common blocks.

The pseudo-code for the subroutine *chfmn* is shown in Fig. 11. This subroutine implements Eq. (100), with the path of integration Γ truncated to the intervals (*-jlower* , *j*0) plus (0 , *upper*).

3. Integrand Implementation

With reference to Fig. 10, the subprograms related to the computation of the integrand are *reinteg*, *iminteg*, *integr*, *refl*, *hwvgky and dbsj0* [1]. They are all implemented as FORTRAN external functions.

The functions *reinteg* and *iminteg* just return the real and imaginary parts of the integrand, respectively. They are called by the integration subroutine, whose first argument is the name of the function to be integrated.

a. Function Integr

The function *integr* computes the (complex) integrand in Eq. (100). The pseudo-code for this function is shown in Fig. 12. The argument k_{y2} is interpreted as imaginary when it has a negative value, in all subprograms. The IF statements marked in the list are related to the medium transfer function. New

---

[1]IMSL, Inc., *DBSJ0, SFUN/Library, Bessel Functions of Integer Order*, 1984.

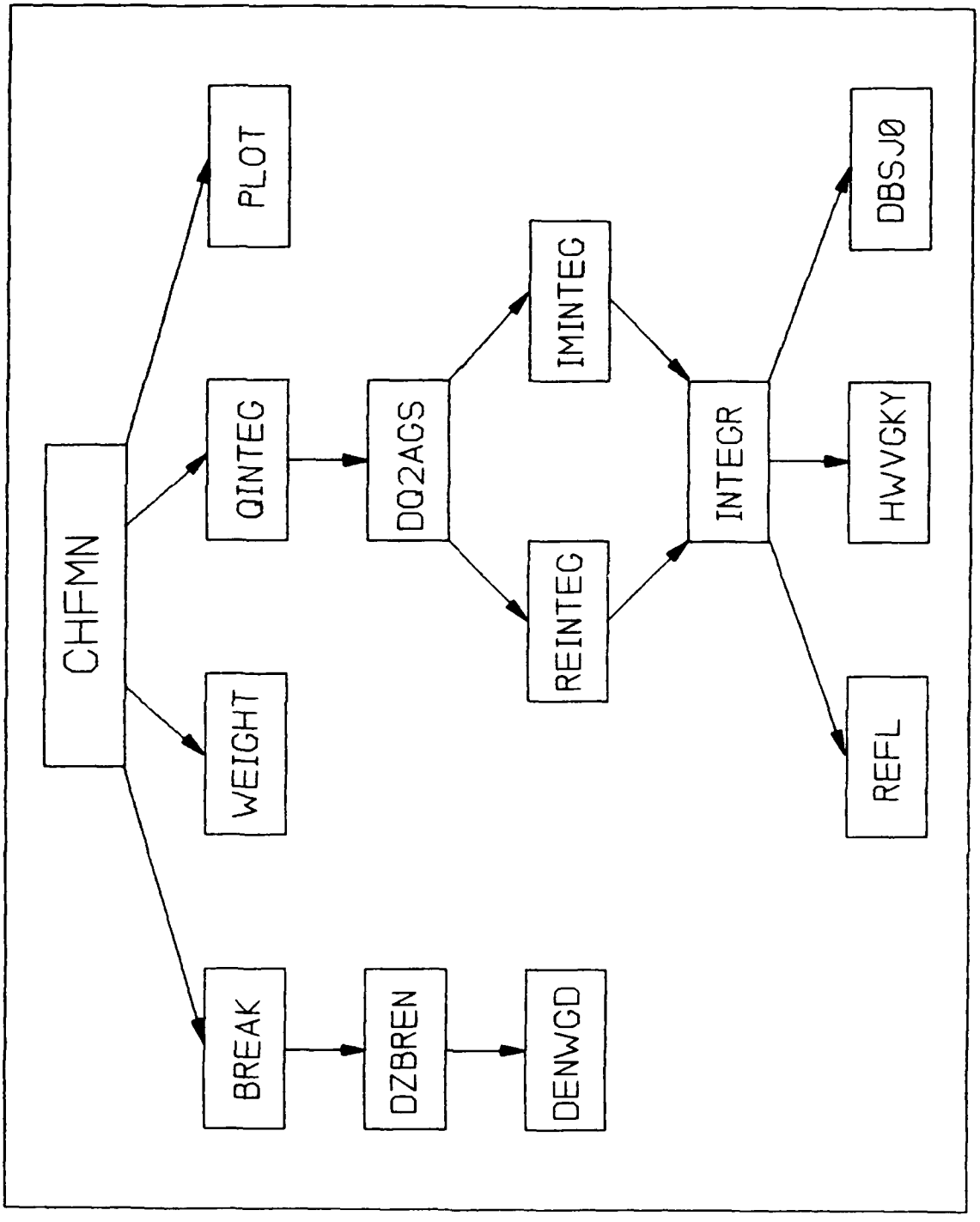

Fig. 10. Structure of the Subroutine *Chfmn*.

```
Subroutine Chfmn
    FOR ( each frequency f= f_c + k f_o ) DO  /-K_max ≤ k ≤ K_max/
        EXECUTE Weight   /compute transmitter array weights c_mn(f)/
        FOR ( each position y_n in receiver ) DO
            EXECUTE Break  /compute breakpoints for integration/
            Compute upper and lower limits of integration
            FOR ( each position x_m in receiver ) DO
                EXECUTE Qinteg(Real part)    /compute Re{ H(f,r_mn) }
                    and its error Re{ EH(f,r_mn) }/
                EXECUTE Qinteg(Imag part)    /compute Im{ H(f,r_mn) }
                    and its error Im{ EH(f,r_mn) }/
                Compute magnitude and phase of H and EH
            END FOR each x_m
        END FOR each y_n
        Plot magnitude and phase of H versus position (x, y)
    END FOR each frequency
End Subroutine Chfmn
```

Fig. 11. Pseudo-Code for the Subroutine *Chfmn*.

Function Integr(k_{y2})

/this function is executed for constant frequency, receiver position (m, n) and k_{y2}/

Compute k_r /Eq. (92)/

IF[1] (layered waveguide) THEN

R_{21} = Refl (surface data) and R_{23} = Refl (bottom data)

END IF

/compute product $\Psi \cdot k_{y2}$, for each y_q, as an array $Ftran(q)$/

FOR (each position y_q in transmitter array) DO

IF[1] (layered waveguide) $Ftran(q)$ = Hwvgky /$k_{y2} \cdot \Psi(f, k_{y2}, y_o; y_n)$/

END FOR each y_q

/compute integrand according to Eq. (100)/

FOR (each position x_p in transmitter array) DO

Compute Bessel function $J_o(k_r R_o)$ /R_o is the horizontal distance from transmitter element to receiver position/

FOR (each position y_q in transmitter array) DO

Acumulate product $c_{pq}(f) \cdot Ftran(q) \cdot J_o(k_r R_o)$ / $\sum_p \sum_q$ /

END FOR each y_q

END FOR each x_p

Integr = (acumulated product)/2π

End Function Integr

[1]Other IF statements may be necessary for different medium transfer functions

Fig. 12. Pseudo-Code for the Function *Integr*.

transfer functions are implemented by adding new IF statements. The functions *integr* and *break*, to be described later, are the only ones that need to be modified when incorporating other medium transfer functions to the program.

b. Function Refl

This function computes the complex reflection coefficients. Its pseudo-code is shown in Fig. 13.

The expressions for both reflection coefficients, Eqs. (73) and (76), can be written as

$$R_{2p} = \frac{\rho_p \; k_{y2} \; - \; \rho_2 \; k_{yp}}{\rho_p \; k_{y2} \; + \; \rho_2 \; k_{yp}}, \tag{121}$$

Function Refl(c_p, c_2, ρ_p, ρ_2, k_{y2})

/computes reflection coefficient R_{2p}/

Compute k_{yp} /Eq. (92)/

IF (the speeds of sound are different) THEN

Compute reflection coefficient by Eq. (121)

ELSE

Compute reflection coefficient by Eq. (122)

END IF

End Function Refl

Fig. 13. Pseudo-Code for the Function *Refl*.

where k_{yp} is given by Eq. (92). If the speed of sound is the same in both media, then Eq. (121) can be simplified to

$$R_{2p} = \frac{\rho_p - \rho_2}{\rho_p + \rho_2}. \tag{122}$$

c. *Function Hwvgky*

The function *hwvgky* returns the complex product $k_{y2}\,\Psi(f, k_{y2}, y_o; y_n)$, the medium dependent factor in the integral expression for the overall transfer function, Eq. (100). This function is specific to the layered waveguide and implements Eq. (81), multiplied by k_{y2}. It is called by the function *integr*, as described earlier (see Figs. 10 and 12). Its implementation is trivial. Its arguments are the frequency, k_{y2} and the y coordinates of the transmitter and receiver array elements, y_q and y_n, respectively. The reflection coefficients R_{21} and R_{23}, and the depth D are available through common blocks.

d. *Examples*

In this section we examine the behavior of the integrand in the expression for the overall transfer function, Eq. (100). In all plots in which k_{y2} is the independent variable, negative values of k_{y2} are imaginary and positive values are real. For simplicity, both negative imaginary and positive real values of k_{y2} are plotted on the same axis. The symbol "□" appearing on the plots is used by the plotting routine to mark different plots on the same graph, but it has no special meaning in the present context.

(1) The Range Factor $J_o(k_r R_o)$. Figures 14 and 15 show the plots of $J_o(k_r R_o)$ vs k_{y2}, which is related to k_r through Eq. (91). The frequency is $f=$

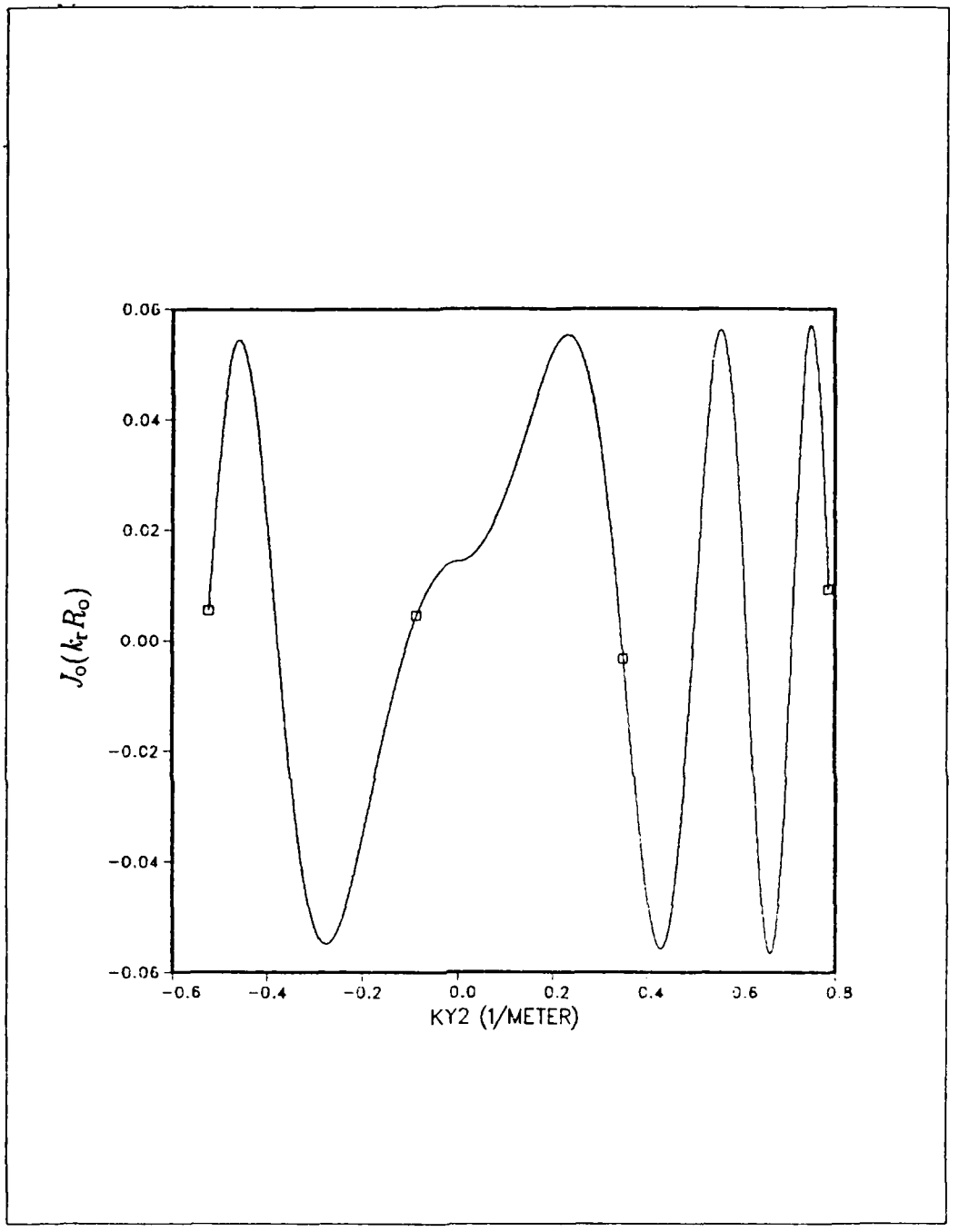

Fig. 14. Range Factor $J_0(k_r R_0)$ for $f = 500$ Hz, $c_2 = 1{,}500$ m/s, and $R_0 = 100$ m.

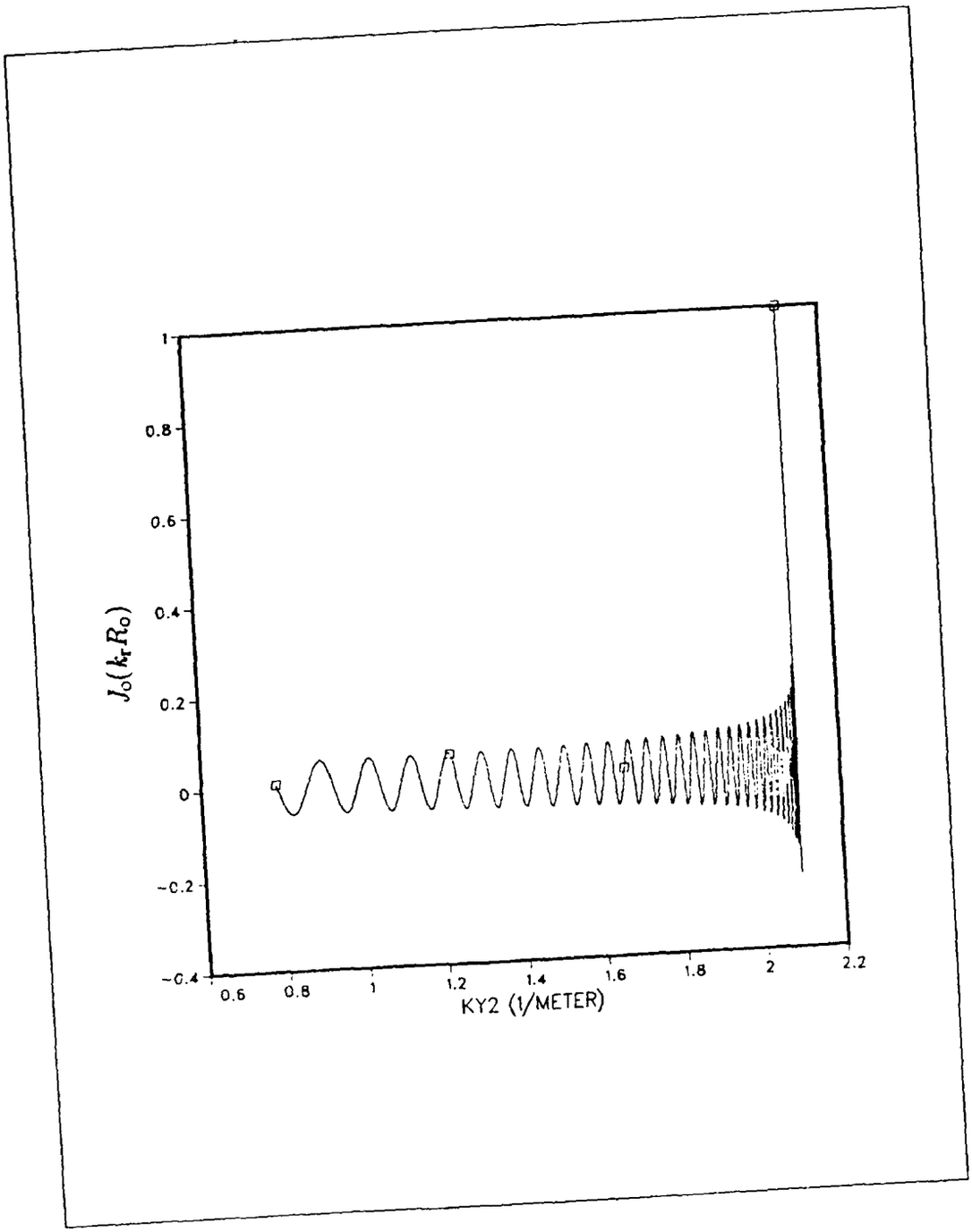

Fig. 14. Range Factor $J_0(k_r R_o)$ for $f = 500$ Hz, $c_2 = 1{,}500$ m/s, and $R_o = 100$ m (cont.).

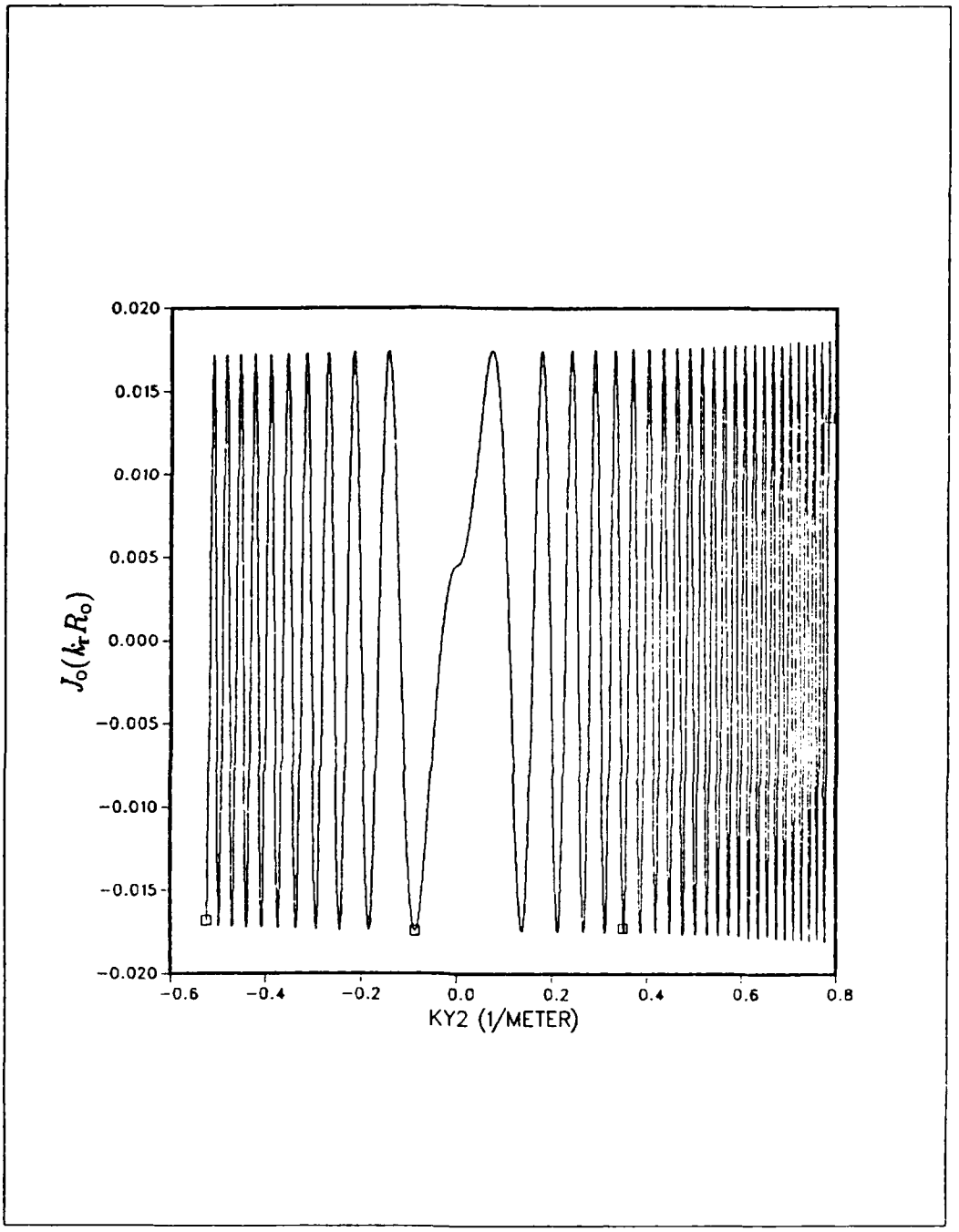

Fig. 15. Range Factor $J_o(k_r R_o)$ for f = 500 Hz, c_2 = 1,500 m/s, and R_o = 1,000 m.

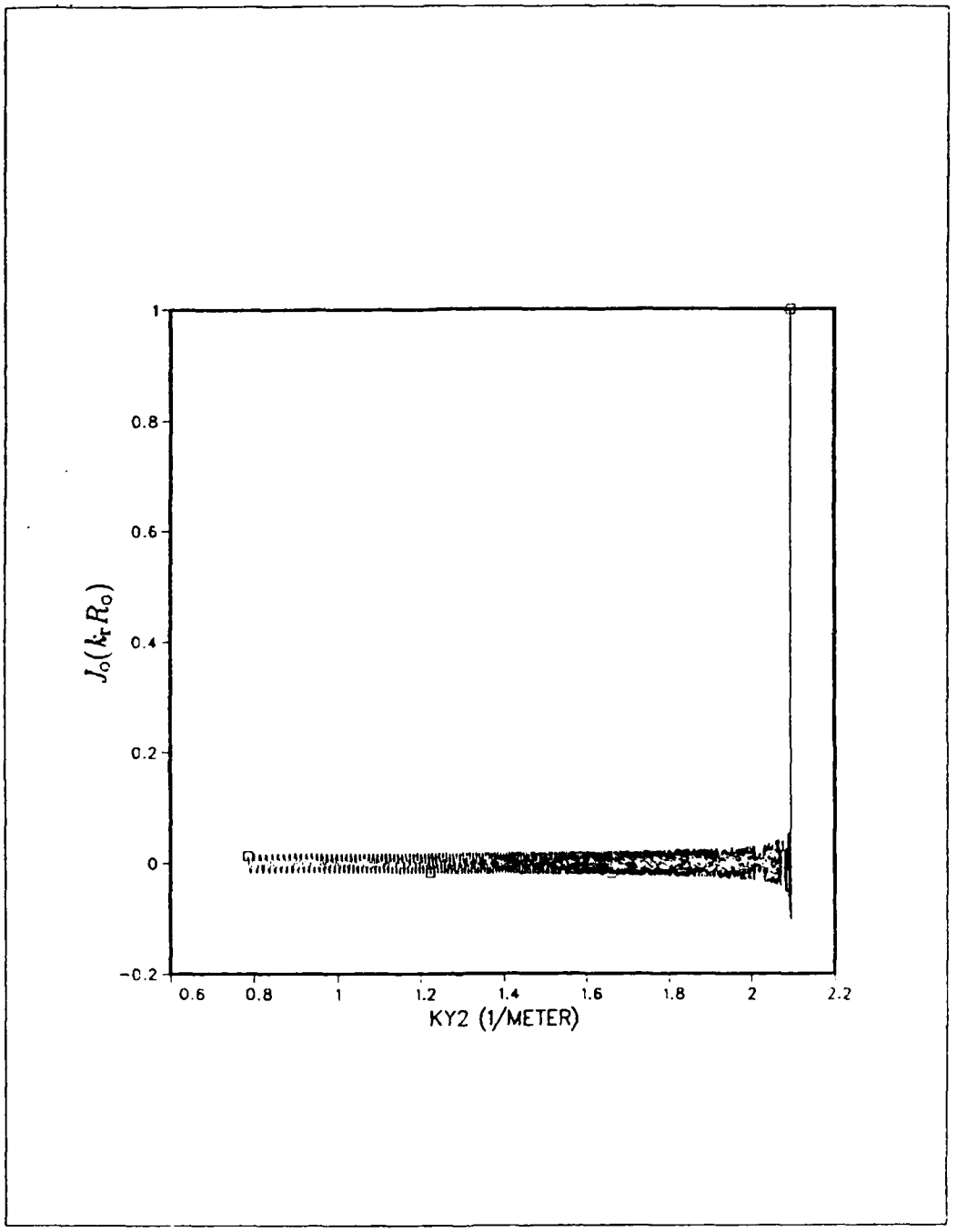

Fig. 15. Range Factor $J_0(k_r R_0)$ for $f = 500$ Hz, $c_2 = 1500$ m/s, and $R_0 = 1000$ m (cont.).

= 500 Hz and the sound speed is c_2 = 1,500 m/s, which results in a wavenumber $k_2 = 2.09\ \mathrm{m}^{-1}$. In Fig. 14, the distance is R_o = 100 m and, in Fig. 15, it is 1,000 m. In those figures the range of k_{y2} is $(-j0.25\ k_2\ ,\ j0)$ plus $(0\ ,\ k_2)$. An important characteristic of the factor $J_o(k_r R_o)$ is that it oscillates slower near $k_{y2} \approx 0$. Another characteristic behavior is that it oscillates faster as the range increases. If the other terms in the integrand also have "slow" oscillations, then the greater contribution for the result of the integration comes from the region $k_{y2} \approx 0$, as a result of the smoothing nature of the integration operation. Physically, the plane waves that travel near the horizontal, that is, those with $k_{y2} \approx 0$, contribute more to the total field than those that interact more with the boundaries. In order to compare the "frequency of oscillations" of the Bessel function and of the medium transfer function, recall that, for $k_r R_o > 2\pi$, the zeros of $J_o(k_r R_o)$ occur approximately at intervals of

$$\delta k_r = \frac{\pi}{R_o}. \tag{123}$$

(2) The Medium Factor. Figure 16 shows the plot of the term $k_{y2}\ \Psi$ for the layered waveguide whose characteristics are shown in Table 1. The depth D of the ocean is 100 m and the frequency is 500 Hz. The position of the point source is $(x_s,\ y_s,\ z_s)$ = (0, 30, 0) meters and the point receiver sensor is at $(x_r\ ,\ y_r\ ,\ z_r)$ = = (1000 ,50 , 0) meters, corresponding to the range factor shown in Fig. 15.

This waveguide is of the almost-pressure-release-surface/fast-bottom type. The peaks are evident in the figures. From the discussion in Section III-A-1b, there are 33 peaks in the range $0 \le k_{y2} \le 1.04\ \mathrm{m}^{-1}$, separated by $\Delta k_{y2} \approx \pi/100$.

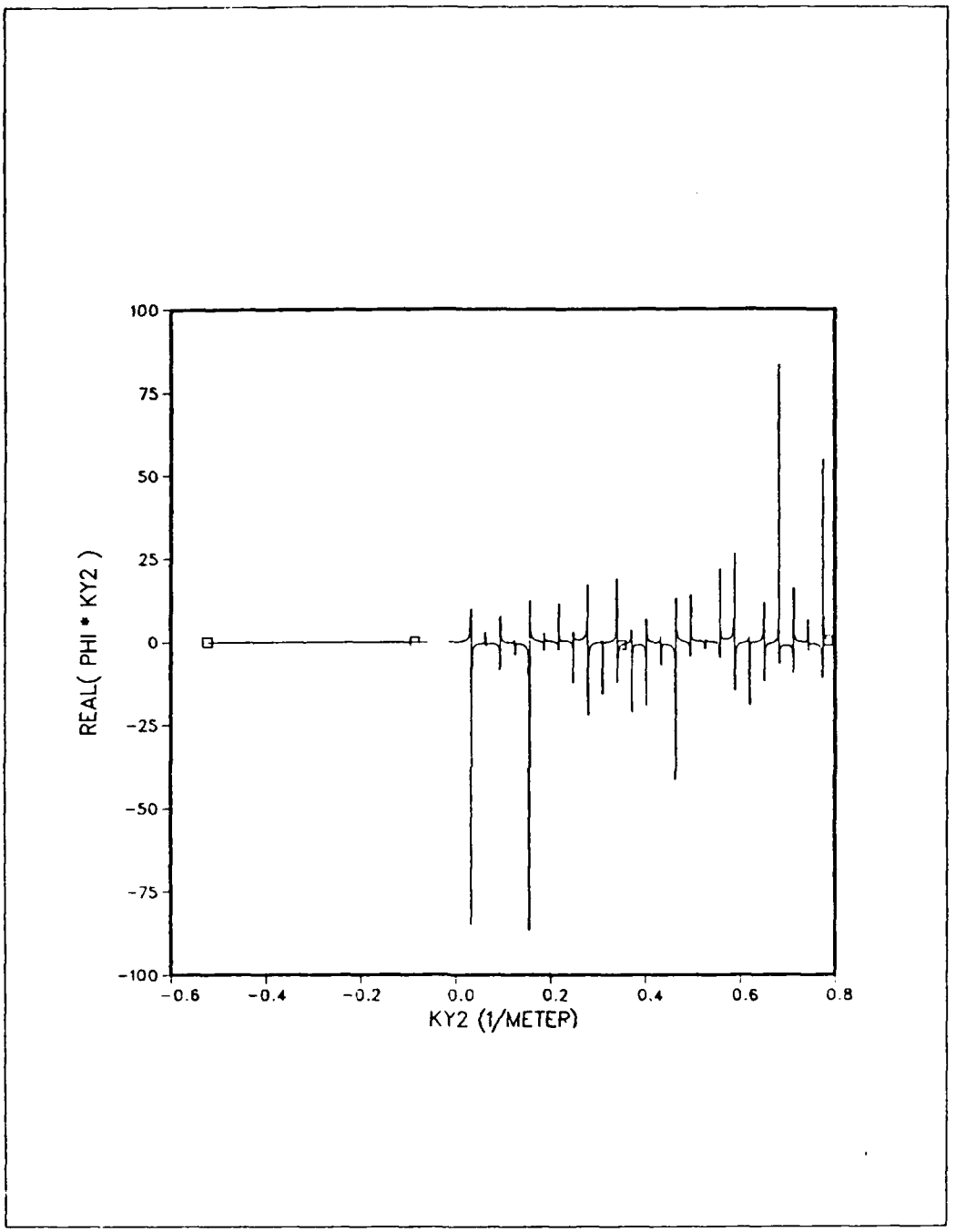

Fig. 16. Waveguide Medium Transfer Function Times k_{y2}. (a) Real Part.

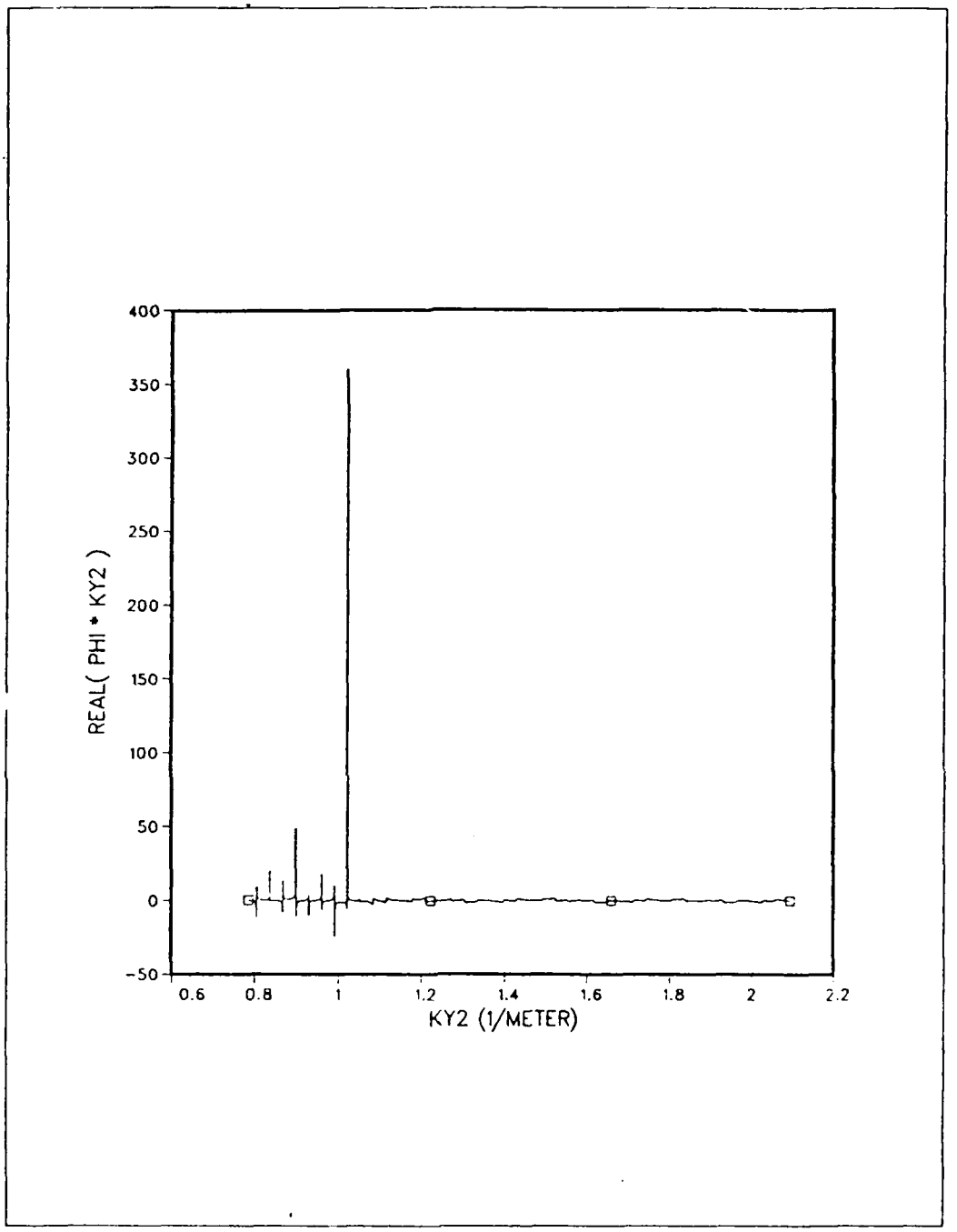

Fig. 16. Waveguide Medium Transfer Function Times k_{y2}. (a) Real Part(cont.).

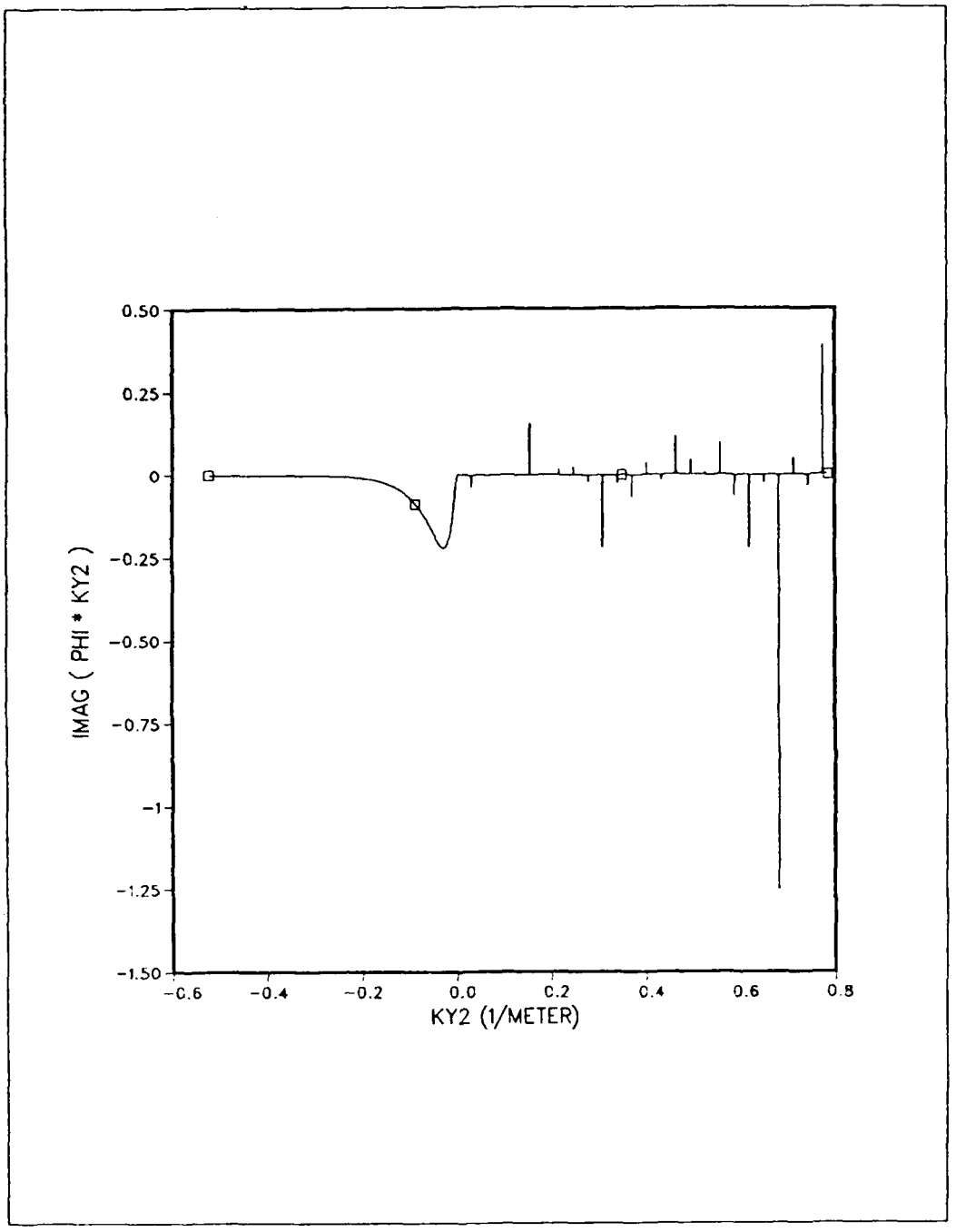

Fig. 16. Waveguide Medium Transfer Function Times k_{y2}. (b) Imaginary Part.

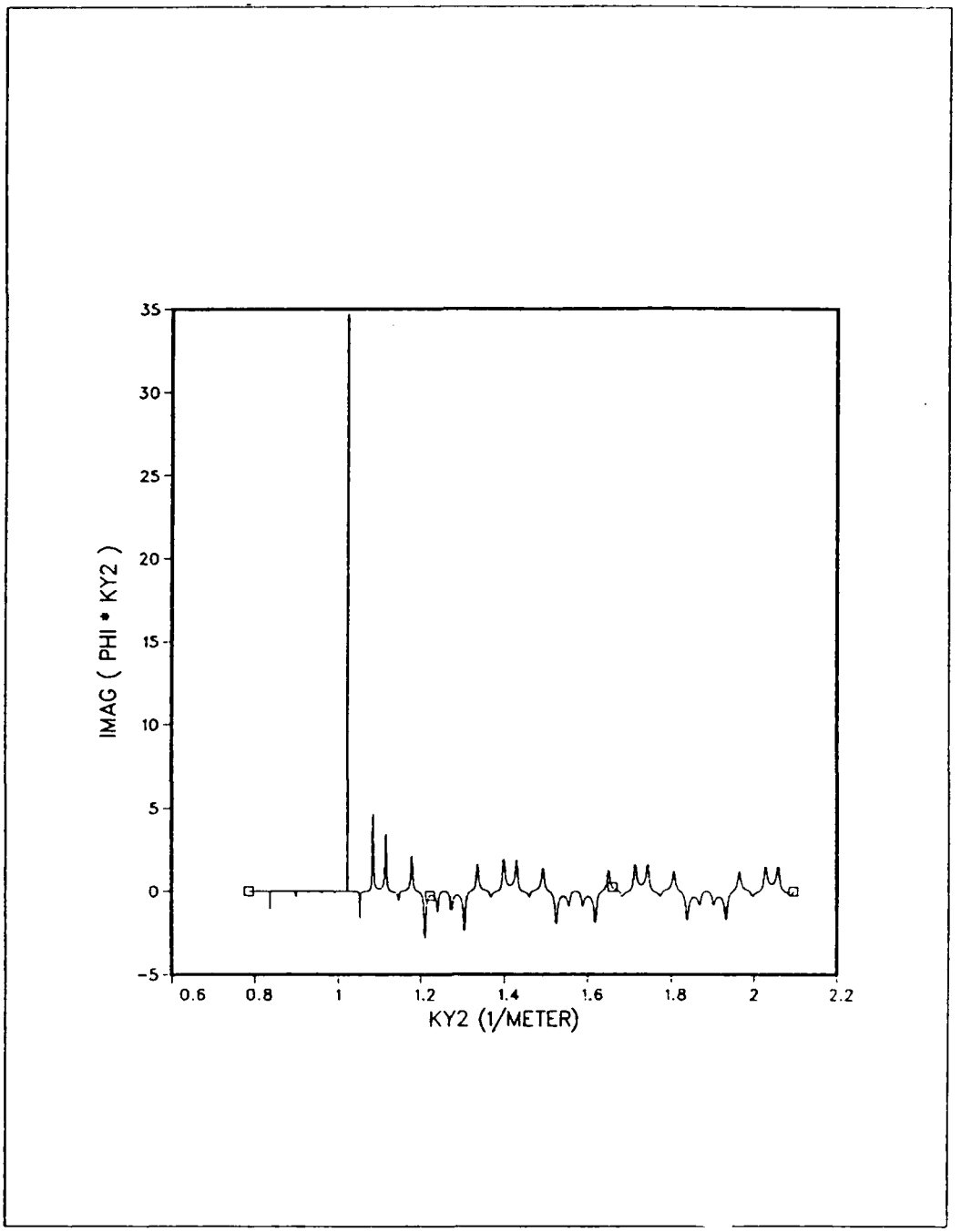

Fig. 16. Waveguide Medium Transfer Function Times k_{y2}. (b) Imaginary Part(cont.).

TABLE 1. WAVEGUIDE ACOUSTIC CHARACTERISTICS

Medium	Speed of Sound ($m\ s^{-1}$)	Density ($Kg\ m^{-3}$)
I	343.0	1.21
II	1500.0	1026.0
III	1730.0	2070.0

A criterion to set an upper limit of integration in Eq. (100)—the *upper* discussed in Section III-B-2—could be based on the comparison between the "periodicities" of the medium and range factors in the integrand. If the factors in the expression for Ψ, Eq. (81), are multiplied out, the faster oscillatory factor—the one with the greater exponent—has a "period" of π/D or more, with respect to k_{y2}, that is,

$$\delta k_{y2} \approx \frac{\pi}{D} . \tag{124}$$

From Eq. (91), the increments δk_{y2} and δk_r are approximately related by

$$|\delta k_r| \approx \frac{k_{y2}}{\sqrt{k_2^2 - k_{y2}^2}} |\delta k_{y2}| , \tag{125}$$

when k_{y2} is real. Equations (123) and (125) can be used to compute the interval between zeros of the range factor, when it is plotted versus k_{y2}. If we require, for example, that the integral be truncated when the Bessel function passes through zero N times during one "period" of the medium factor, then, substituting Eq. (123) and $\delta k_{y2} = \pi / ND$ into Eq. (125), yields

$$upper = \frac{k_2}{\sqrt{1 + (R_o / ND)^2}} . \tag{126}$$

The upper limit computed according to Eq. (126) can smaller than the last peak position, given by $\sqrt{k_2^2 - k_3^2}$ [see discussion following Eq. (99)]. In this case, the limit could be increased, or those peaks outside the limit could be simply discarded. In this implementation, the *upper* limit is set to k_2.

The lower limit of integration, in the region where k_{y2} is imaginary negative and $| k_{y2} \cdot \Psi |$ decreases exponentially as $k_{y2} \rightarrow -j\infty$, should be set to minimize the error of integration for the slower decaying factor in $k_{y2} \cdot \Psi$—the one with the exponent of smallest absolute value. The worst case is when there is one constant term, which happens when the source and the receiver are at the same depth, for example. Note that the term $k_{y2} \cdot \Psi$ is pure imaginary when k_{y2} is negative imaginary, and decreases towards zero as $e^{-|k_{y2}| y_o} = e^{-20|k_{y2}|}$. The *lower* limit is set to $-j0.125\ k_2$ in this implementation.

(3) The Integrand. Figure 17 shows the plot of the integrand for the waveguide discussed above, at $f = 500$ Hz, for a range $R_o = 1{,}000$ m. For k_{y2} greater than about 1.5, corresponding to $N \approx 10$ in Eq. (126), the integrand is fairly symmetrical around zero, suggesting a low value for the integral in that region.

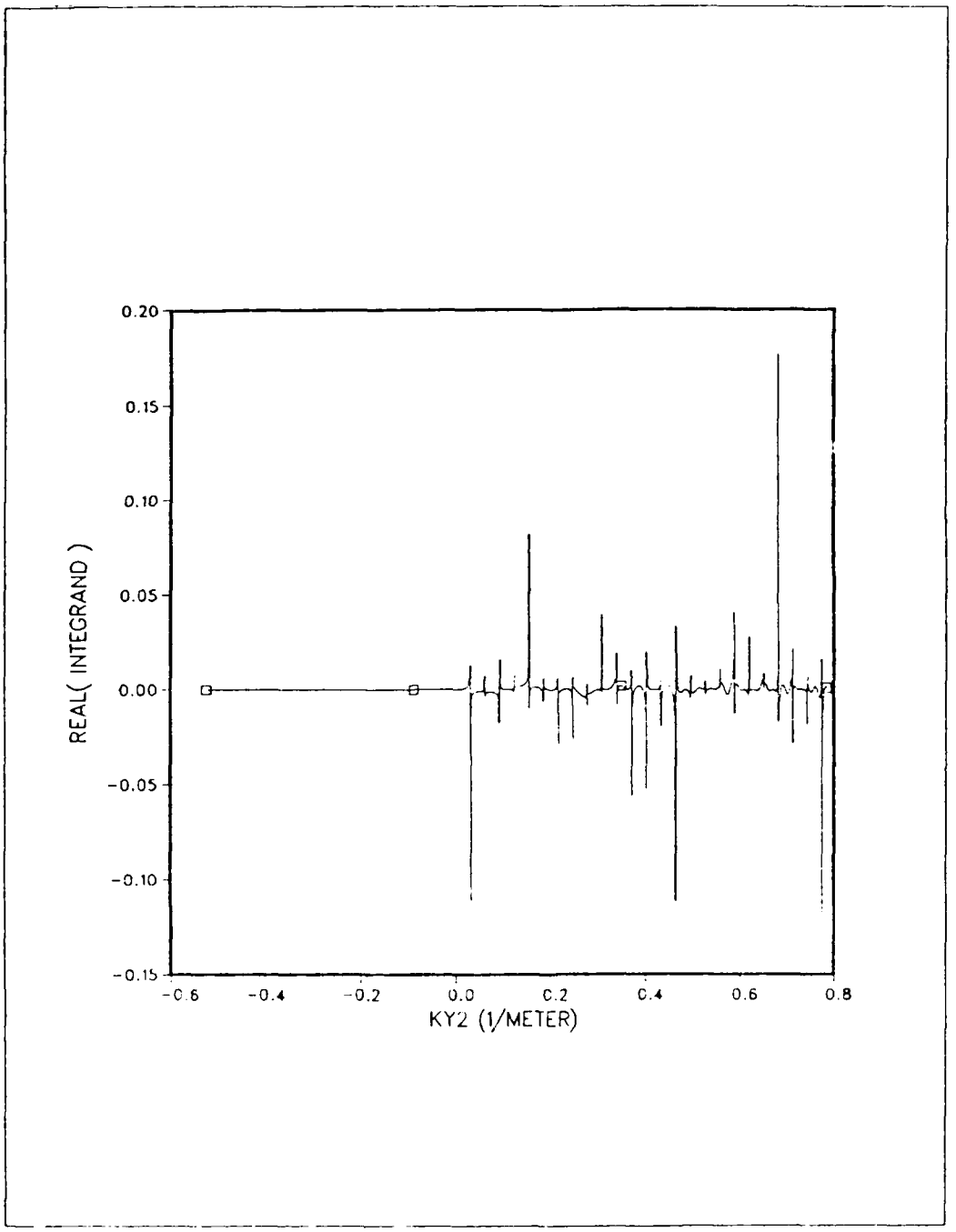

Fig. 17. Waveguide Integrand, Range R_c = 1,000 m. (a) Real Part.

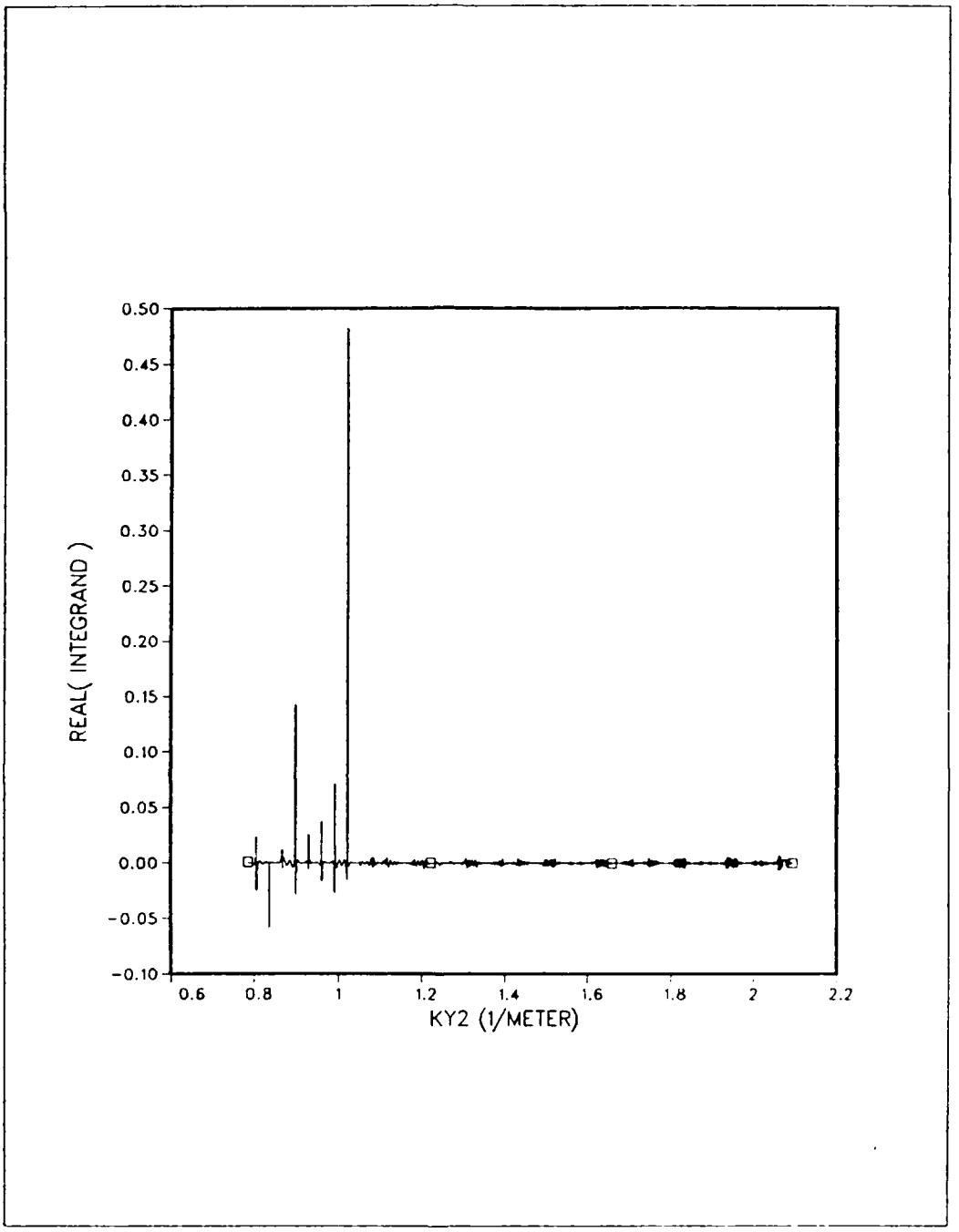

Fig. 17. Waveguide Integrand, Range R_o = 1,000 m. (a) Real Part(cont.).

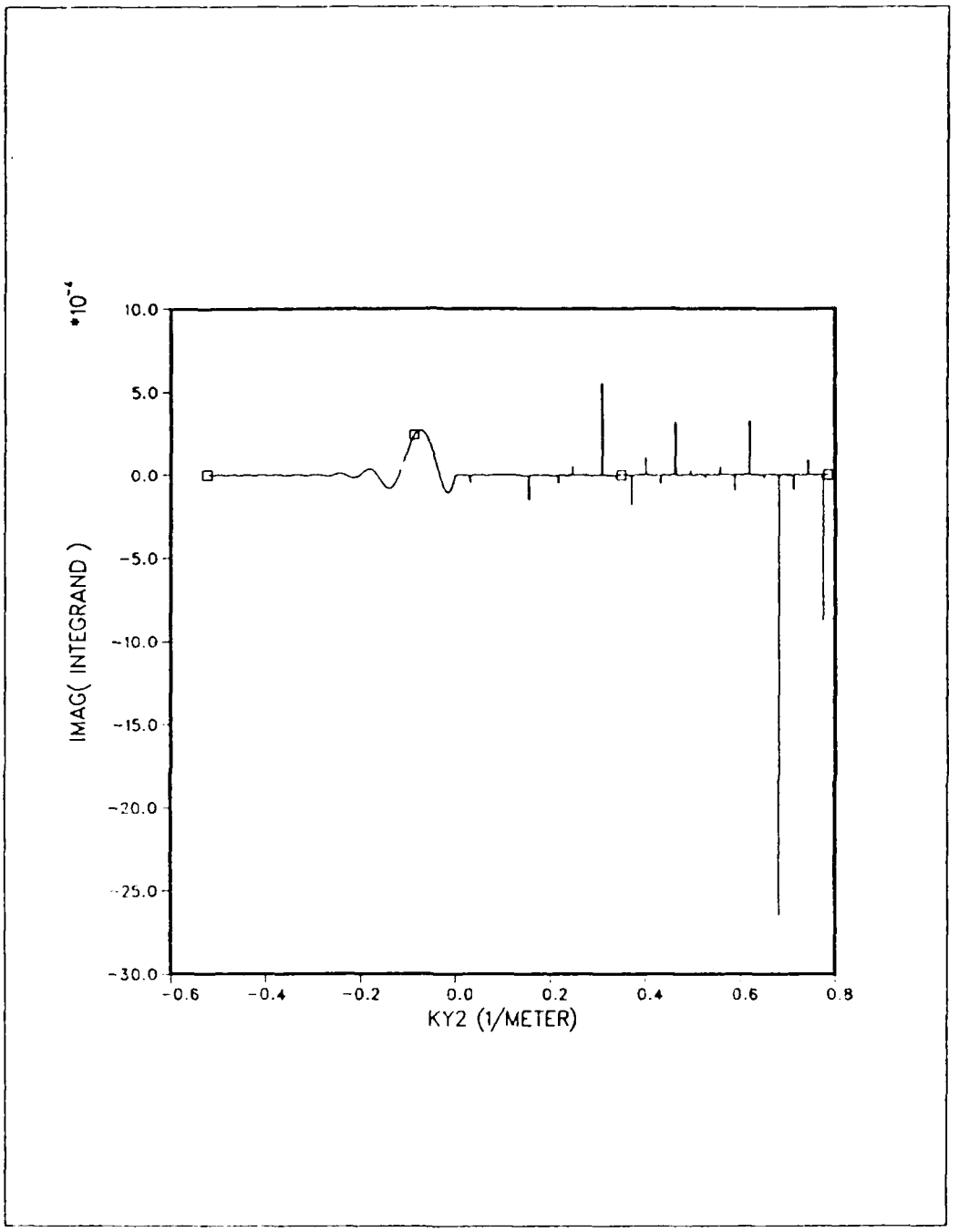

Fig. 17. Waveguide Integrand, Range $R_0 = 1{,}000$ m. (b) Imaginary Part.

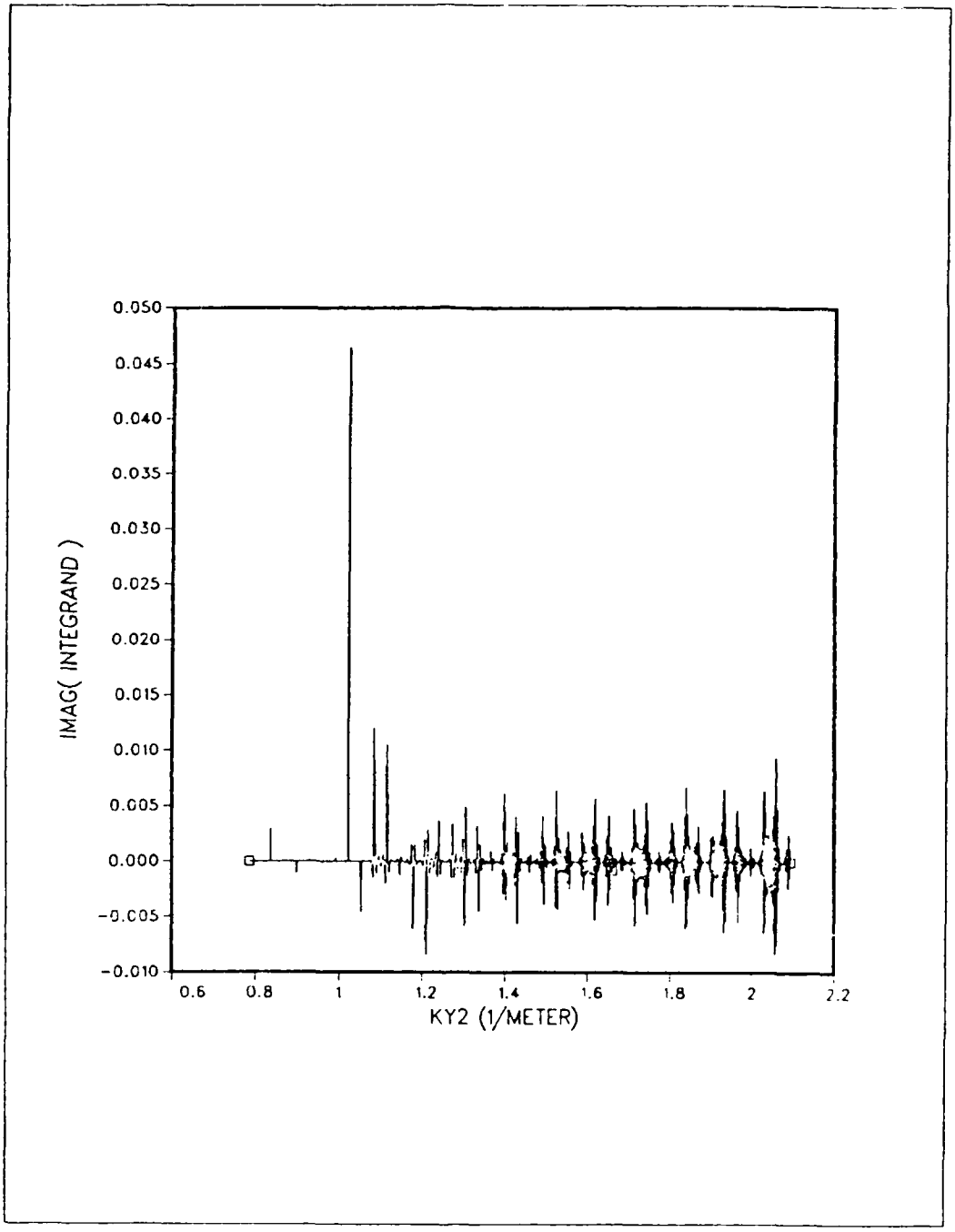

Fig. 17. Waveguide Integrand, Range R_o = 1,000 m. (b) Imaginary Part(cont.).

4. Other Subroutines

a. Subroutine Break

This subroutine divides the interval of integration in order to decrease the error of the integration subroutine. The criteria used in this division are the behavior of the medium transfer function and the relationship between the "periodicities" of that function and of the Bessel function in the integrand. For each different medium transfer function, a different interval subdivision strategy must be implemented. The *upper* and *lower* limits of integration are independent of the type of medium, in this implementation. Nevertheless, they could be made medium dependent, in which case their computation should be included in the subroutine *break*. Figure 18 lists the pseudo-code for this subroutine.

In the case of the layered waveguide function, the breakpoints are set equal to the locations of the peaks, if any, as discussed in Section III-A-1b, regarding the almost-pressure-release-surface/fast-bottom. The interval of values of k_{y2} outside the range of the peaks is divided evenly into subintervals of size $5\pi / D$, corresponding to five "periods," as given by Eq. (124).

(1) Subroutine Description. The input parameters for the subroutine *break* are the frequency f, the speed of sound c_2—computed in the subroutine *chfmn* and taking into account the gradient of the speed of sound, for the case of other media. Other variables shared through common blocks are the type of medium, *OCNTF*, and the waveguide characteristics. The outputs are the number of breakpoints and a vector with the values of k_{y2} at the breakpoints.

Initially, the subroutine divides the interval of integration evenly. Then, it proceeds to check for the presence of peaks in the medium transfer function as discussed in Section III-A-1b. The peaks are the zeros of Eq. (99),

```
Subroutine Break(f, c2 , breakpoints , number_brkpts)
    IF[1] (layered waveguide) THEN
        /divide range evenly (-0.125 k2, 0) U (0, k2)/
        number_brkpts = (1.125 k2 ÷ Δky2) - 1
        FOR (n = 1 to number_brkpts) DO
            breakpoints(n) = (-0.125 k2) + n Δky2
            IF (breakpoints(n) ≤ 0)  index = n    /index keeps track of
                last nonpositive element of vector breakpoints/
        END FOR n
            /check for presence of peaks/
        IF (peaks do exist) THEN   /a > π÷2 , see Eq. (99)/
            /the peaks are located at ky2 = θn÷D, see Eq. (99)/
            number_peaks = ⌈(a/π) - 0.5⌉   / discussion after Eq. (99)/
            FOR (n = index+1 to index+1+ number_peaks) DO
                Compute n_th_zero of the function Denwgd
                breakpoints(n) = n_th_zero ÷ D
            END FOR n
            Update number_brkpts to reflect total number of breakpoints
        END IF
    END IF
End Subroutine Break
```

[1]Other IF statements may be necessary for different medium transfer functions

Fig. 18. Pseudo-Code for the Subroutine *Break*

implemented as the FORTRAN external function *denwgd*. The zeros are found by the subroutine *dzbren*[1]. The (positive) breakpoints originally computed are changed to the values of the positions of the peaks. This implementation assumes a *lower* limit of integration of $-j0.125\ k_2$ and an *upper* limit equal to k_2.

b. Subroutine Weight [2]

The subroutine *weight* computes the transmitter array complex weights $c_{pq}(f)$. The input parameters are the frequency; the transmitter array data; the direction cosines u' (with respect to the X direction) and v' (with respect to the Y direction) of the transmitter array main lobe; the speed of sound at the center of the array—set to c_2 for the layered waveguide, but included in the present implementation to allow for other media—and the gradient of the speed of sound—set to zero in this implementation. The complex weights are given by [Ref. 5:p.133]

$$c_{pq}(f) = a_{pq}\, e^{j\theta_{pq}}\,, \tag{127}$$

where

$$a_{pq} = A_p\, B_q\,, \tag{128}$$

$$\theta_{pq} = \frac{-2\pi}{\lambda}\,(u'\ p\ d_{xt} + v'\ q\ d_{yt})\,, \tag{129}$$

---

[1]IMSL, Inc., *DZBREN, MATH/Library, Nonlinear Equations*, 1985.

[2]This implementation is based on a program originally written by Dr. Lawrence J. Ziomek, at the Naval Postgraduate School.

$$\lambda = \frac{c_2(y_q)}{f}, \tag{130}$$

A_p and B_q are the amplitude weights along the X and Y directions, respectively, λ is the (depth-dependent) wavelength, d_{xt} and d_{yt} are the interelement spacing along the X and Y directions, respectively, and $c_2(y_q)$ is the speed of sound at the depth y_q.

*c. **Subroutine Qinteg***

The subroutine *qinteg* is an interface for the subroutine *dq2ags*[1], which actually performs the integration in Eq. (100). The input arguments are the name of the external FORTRAN function to be integrated, the limits of integration, the breakpoints, the number of breakpoints, and the required error in the result. The output arguments are the result of the integration and its estimated error.

Initially, each interval of integration, defined by the breakpoints, is subdivided in order to improve the convergence of the subroutine *dq2ags*, which is called by *qinteg* to perform each intermediate integration. If the error of the integration of a subinterval, as computed by *dq2ags*, exceeds the requirements, that subinterval is further subdivided. Finally, the results and errors of integration provided by *dq2ags* are accumulated.

As indicated in the pseudo-code of the subroutine *chfmn*, Fig. 11, each

---

[1]IMSL, Inc., *DQ2AGS, MATH/Library, Integration and Differentiation*, 1985.

integration is performed twice, for the real and imaginary parts of the integrand. In terms of computing time, this is the most critical section of code. Not only does the subroutine *qinteg* calls *dq2ags* many times—at least ten times between breakpoints, in the present implementation—but, what is worse, *dq2ags* can execute the function to be integrated, ultimately *integr*, hundreds of times. The computation .ime increases with frequency and range:

- The interval of integration increases as $O(k_2)$, directly proportional to frequency.
- As the range increases, the range factor $J_0(k_r R_0)$ oscillates faster, degrading the convergence of the integration subroutine, causing more executions of the function *integr* and more frequent interv .l subdivisions.

The effect of range can be minimized if the limits of integration, *lower* and *upper*, decrease (in absolute value) with range, as in Eq. (126) for the upper limit.

C. RESULTS

The algorithms described in the previous section are tested by using two examples for which the results are easily interpreted. The unbounded homogeneous medium was presented in Section II-C-3a as a particular case of the layered waveguide, all three media with the same acoustic characteristics. The surface reflection problem was analyzed in Section II-C-3b. In both cases, the input to the system is a time-harmonic point source and the output electrical signal—numerically equal to the velocity potential—is given by Eqs. (85) and (88). From Ec 40c). the time-independent term of the output signal is, for a time-harmonic input, equal to the overall transfer function, that is,

$$y_{mn}(t) = \int_{-\infty}^{\infty} X(f)\, H(f,r_{mn})\, e^{j2\pi f t}\, df, \tag{40c}$$

$$y_{mn}(t) = \int_{-\infty}^{\infty} \delta(f-f_o)\, H(f,r_{mn})\, e^{j2\pi f t}\, df, \tag{131a}$$

$$y_{mn}(t) = H(f_o,r_{mn})\, e^{j2\pi f_o t}. \tag{131b}$$

Therefore, the magnitude of the overall transfer function is equal to the magnitude of the velocity potential.

Results for the waveguide example used so far (see Table 1) are also presented.

1. Homogeneous Medium

Figure 19 presents the plot of the magnitude of the overall transfer function as a function of horizontal distance r from the source. The acoustic characteristics are those shown in Table 1 for medium II. The depth of the source is 30 m and of the receiver array, 50 m. The expected result is a straight line on a log-log plot, corresponding to a velocity potential proportional to the inverse of distance. At 100 m, the error of the computed value is 6%, and increases with distance up to 29% at 3,100 m. The integration routine computed the integrand 3,360 times (total for real and imaginary parts) for 100 m of distance, a number that increased to 34,776 at 3,100 m, indicating an increased difficulty in convergence of the integral. An analogous computation for the layered waveguide took 45,000 and 70,000 computations of the integrand, for 100 m and 3,100 m, respectively.

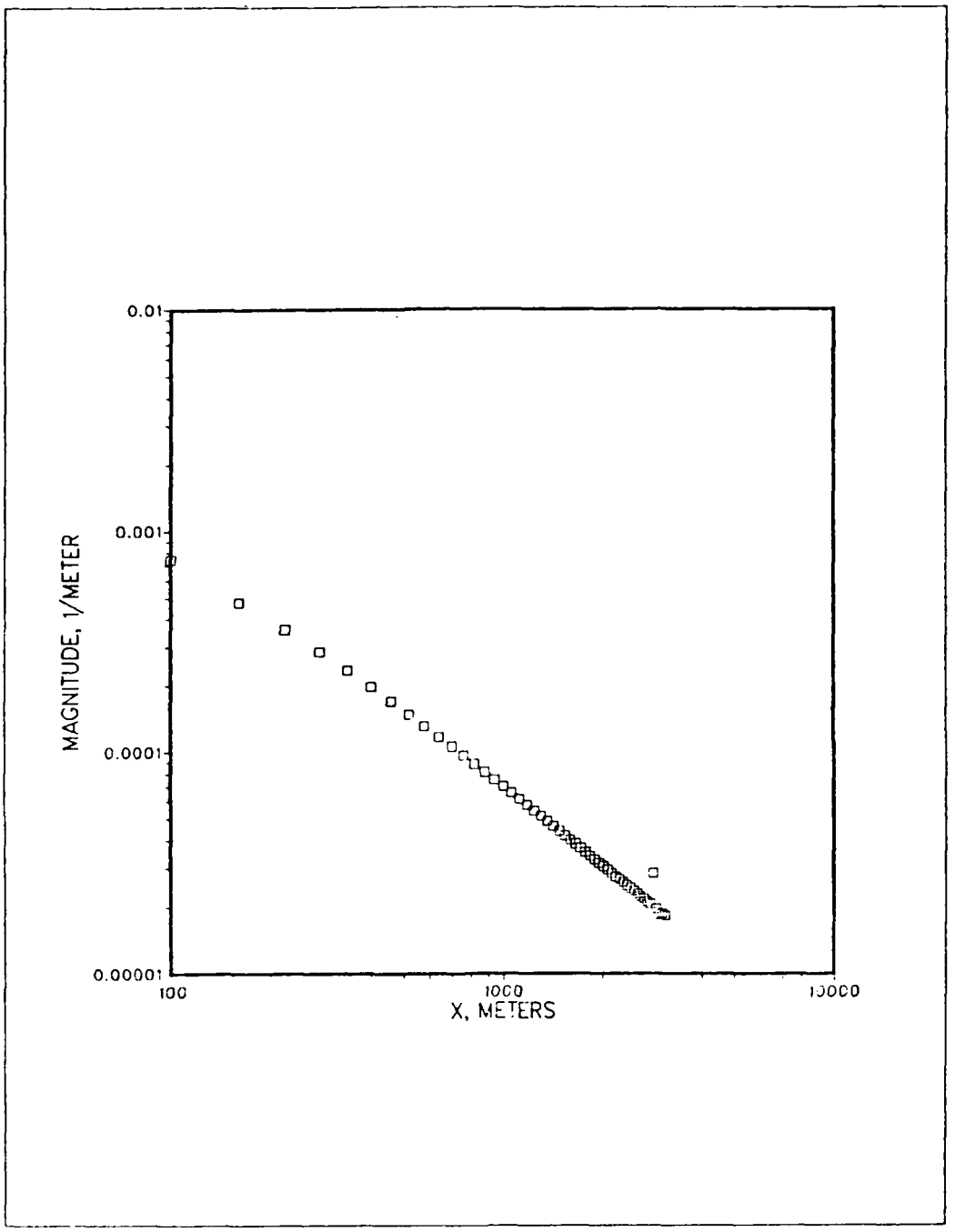

Fig. 19. Overall Transfer Function for a Homogeneous Medium.

2. Surface Reflection

Figure 20 shows the overall transfer function as a function of depth, for a distance of 1,000 m between source and receiver. The acoustic characteristics of the two media are those shown in Table 1 for media I and II. The surface is, for all practical purposes, pressure release. The depth of the source is 30 m. For these data, the approximations for Eq. (89) are valid, indicating a sinusoidal variation with depth. The error increases from zero at the surface, up to a maximum error at 30 m, the depth of the source—see discussion in Section III-B-3d, regarding the lower limit of integration. At 30 m, near a theoretical maximum, the error is 45% . At depths greater than 60 m, the error is negligible. For comparison purposes, the integrand was computed about 11,000 times for each value of the overall transfer function.

3. Layered Waveguide: Waveform Prediction

Figure 21 shows the transmitted signal. This signal was obtained by truncating the Fourier series of a CW pulse, as explained in Section III-B-1a. The reference signal is a rectangular-envelope CW pulse of duration 20 ms and repetition period of 400 ms. The carrier frequency is f_c = 500 Hz Seventeen frequency components are used for the transmitted signal, that is, K_{max}= 8. The resultant bell-shaped CW pulse has a duration of 100 ms. Ringing is barely visible, due to the low sidelobes of the Hamming window used for the truncation of the Fourier series. The extension of time in the plot of Fig. 21 is equal to one period.

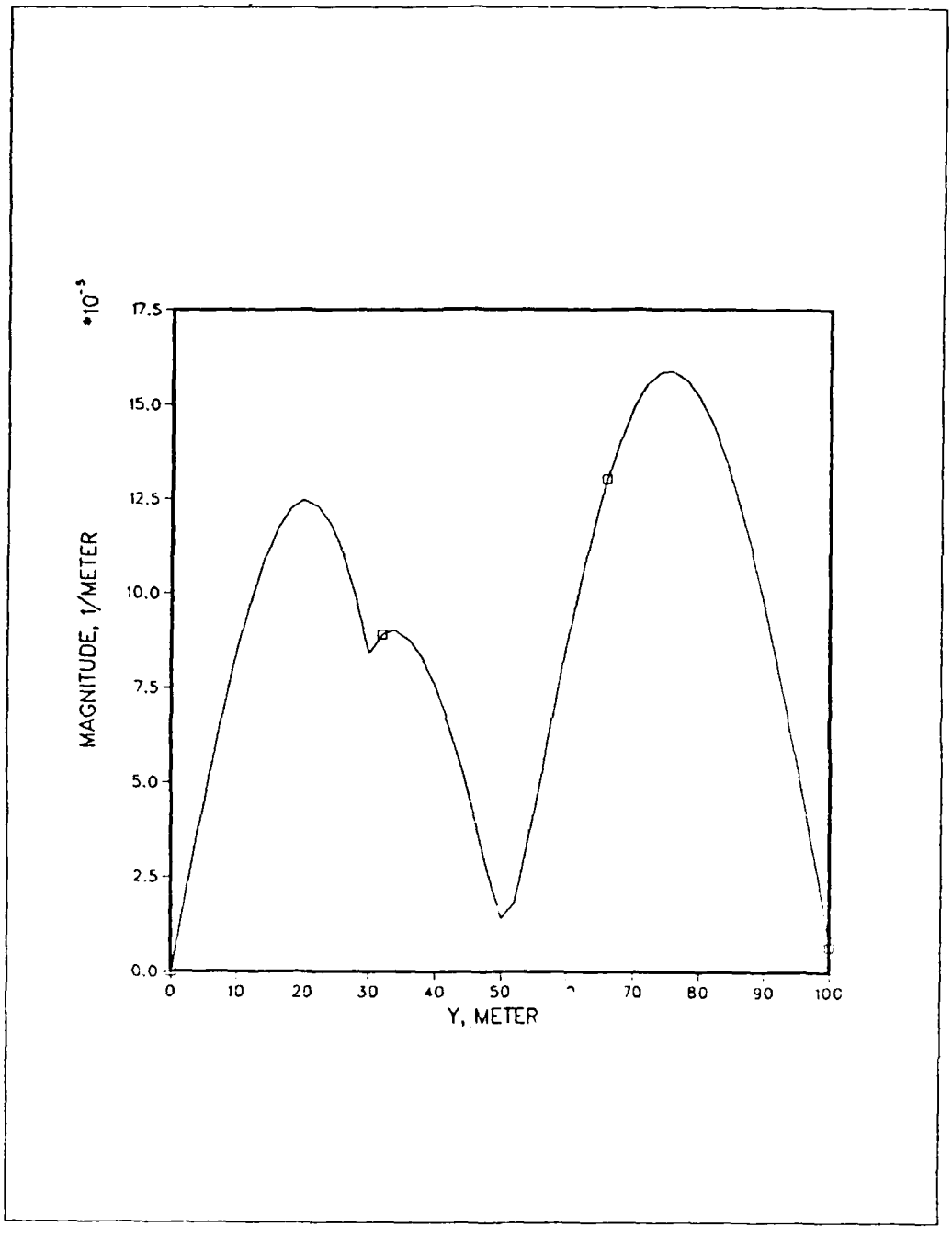

Fig. 20. Overall Transfer Function for the Surface Reflection Problem.

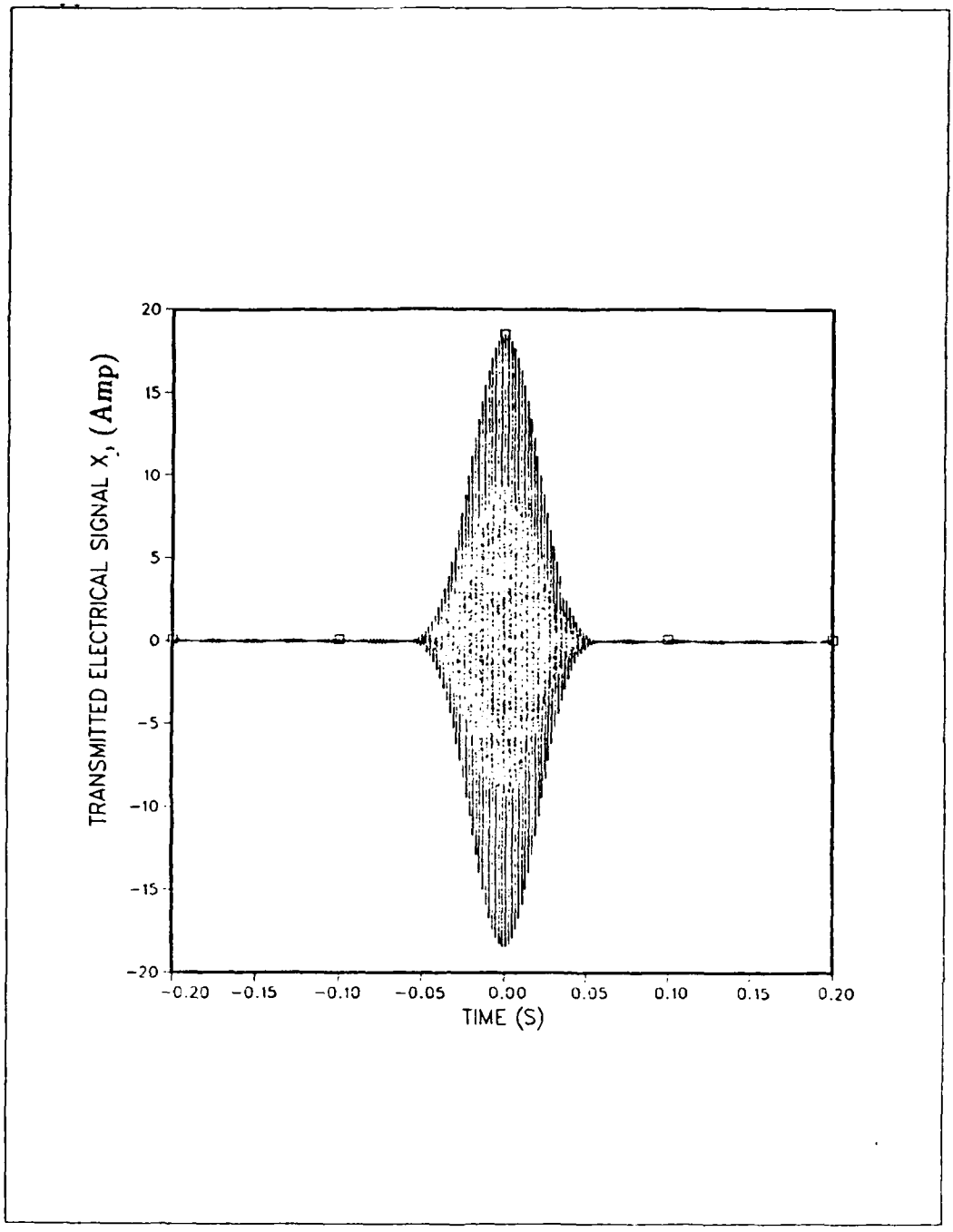

Fig. 21 Transmitted Signal.

The acoustic characteristics of the media are the same as for the examples in Section III-B-3d and are listed in Table 1. The distance is R_o = 1,000 m. The transmitter is located at (x_s, y_s, z_s) = (0, 30, 0) meters, and the receiver at (x_r, y_r, z_r) = (1000, 50, 0) meters.

Figure 22 shows the received pulse when the transmitter is a single point source. The distortion due to the multipath nature of the medium is evident.

Figure 23 shows the received pulse due to a 5 × 5 transmitter array. The interelement spacing is roughly $\lambda/2$ in both the X and Y directions. Note that the pulse arrivals occur at the same instants as in Fig. 22, but the relative amplitudes are different.

D. CONCLUSIONS

The equations that describe a range-independent acoustic communication channel were derived by using linear systems theory, a basic engineering tool, as a framework. They incorporate aspects of signal processing and acoustic propagation. The main results from Chapter II are the expression for the overall transfer function, Eq. (51) or its alternative form, Eq. (60); and the procedure to obtain the transformed medium transfer function, the solution to the inhomogeneous Helmholtz wave equation, Eq. (90). These results, together with Eq. (40c), were used to implement a waveform prediction program, as described in Section III-B. We do not claim novelty of results. Equation (60) is a mere extension of a classical result, in which the contributions of the point sources that make up an array are

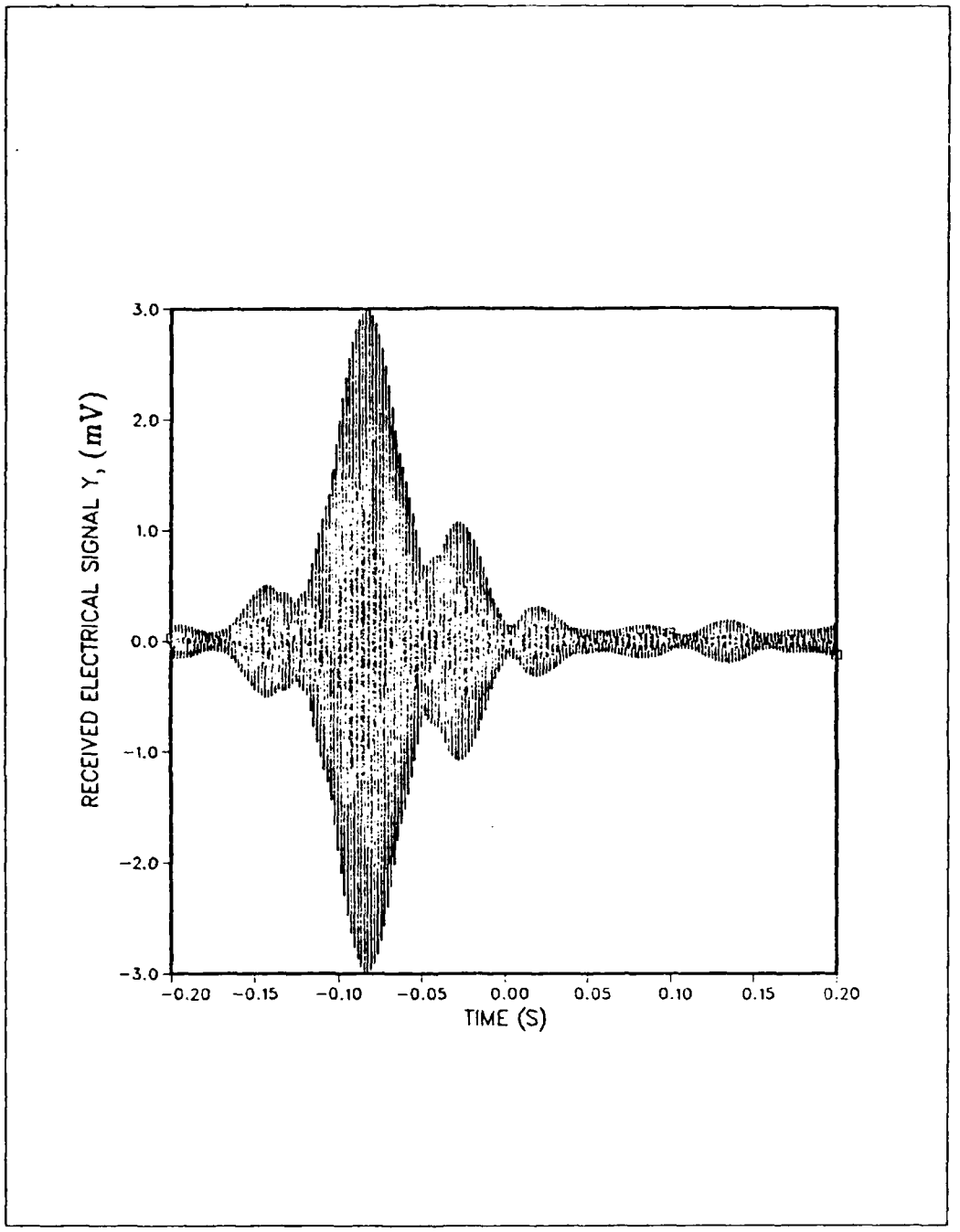

Fig. 22. Output Electrical Signal Due to a Single Point Source.

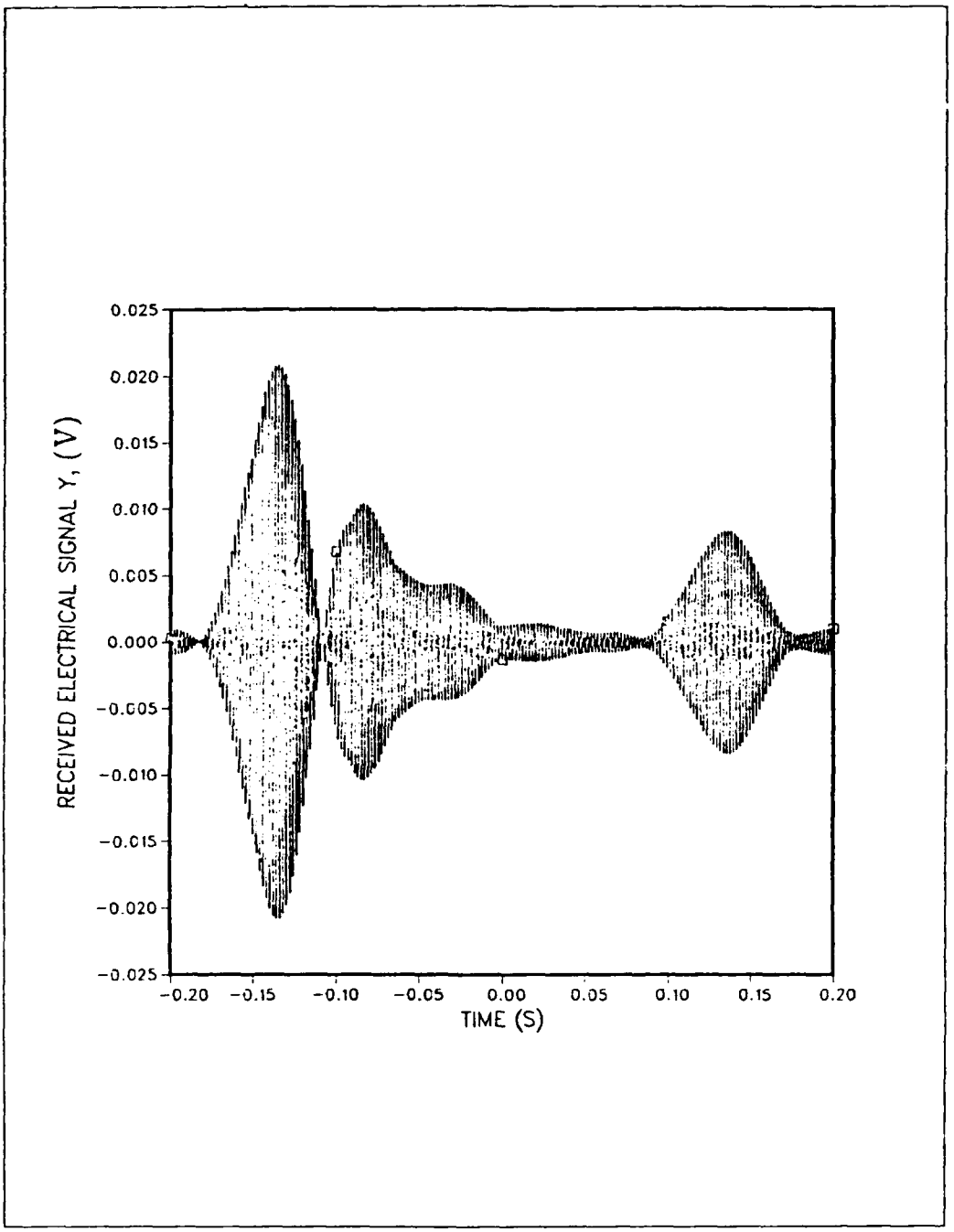

Fig. 23. Output Electrical Signal Due to a 5×5 Transmitter Array

simply added, a consequence of the linearity of the wave equation that describes small-amplitude acoustic phenomena. The medium transfer function for the layered waveguide was derived in order to enable us to implement a working computer program.

The program described in Section III-B is based on a slightly modified form of Eq. (60), in which we use the wavenumber y-component k_{y2} as the independent variable. The only justification for this change of variable is the easier analysis of the medium transfer function. The program works, but is slow. The computation of the waveform shown in Fig. 23, for example, took about three minutes per frequency component, with an overhead time—independent of the number of frequency components—of about two minutes, in an IBM 3033U/4381 2-cpu network. Both the speed and accuracy can be improved by using an adaptive technique for the truncation of the interval of integration, that is, computation of the limits of integration as a function of the behavior of the medium and range factors in the integrand.

Other implementations are possible, for example, the Fast-Field-Program described in [Ref. 4:pp. 90-92]. Equation (51), in the form of a two-dimensional Fourier transform, could be useful for implementation.

Concerning the medium transfer function, analytical solutions to the range-independent wave equation are only available for a few speed-of-sound profiles. Approximate solutions, like those provided by the WKB method, are candidates for implementation. On the other hand, numerical methods may not be feasible for our purpose, waveform prediction, due to time constraints.

As mentioned in the beginning of Chapter III, the main thrust for the present implementation of the range-independent equations was to have a working program. The program is working. More than an improvement, it possibly needs a different implementation. Nevertheless, the basic important fact is that, independent of the implementation, the modular nature of the equations should be fully exploited. Solutions to specific problems can be implemented by adding new subprograms, with a minimum of code change. Further investigation is recommended.

LIST OF REFERENCES

1. Ziomek, L. J., and Blount, R. J., Jr., "Underwater Acoustic Model-Based Signal Processing," *IEEE Transactions on Acoustics, Speech and Signal Processing*, v. ASSP-35, pp. 1670-1683, December 1987.

2. Baggeroer, A. B., Kuperman, W. A., and Schmidt, H., "Matched Field Processing: Source Localization in correlated Noise as an Optimum Parameter Estimation Problem," *Journal of the Acoustic Society of America*, v. 83, pp. 571-587, February 1988.

3. Officer, C. B., *Introduction to the Theory of Sound Transmission With Application to the Ocean*, McGraw-Hill Book Company, Inc.,1958.

4. DiNapoli, F. R., and Deavenport, R. L., "Numerical Models of Underwater Acoustic Propagation," in *Ocean Acoustics*, ed. by J. A. DeSanto, Topics in Current Physics, Vol. 8, Springer-Verlag, 1979.

5. Ziomek, L. J., *Underwater Acoustics—A Linear Systems Theory Approach*, Academic Press, 1985.

6. Mathews, J., and Walker, R. L., *Mathematical Methods of Physics*, 2d ed., Benjamin/Cummings Publishing Company, 1970.

7. Ziomek, L. J., "Lecture Notes—EC 3450: Acoustic Field Theory," Naval Postgraduate School, 1987, unpublished.

8. Kinsler, L. E., and others, *Fundamentals of Acoustics*, 3d ed., John Wiley & Sons, Inc., 1982

INITIAL DISTRIBUTION LIST

1.	Defense Technical Information Center Cameron Station Alexandria, VA 22304-6145	2
2.	Library, Code 0142 Naval Postgraduate School Monterey, CA 93943-5002	2
3.	Chairman, Code 62 Departament of Electrical and Computer Engineering Naval Postgraduate School Monterey, CA 93943-5000	1
4.	Dr. Antony A. Atchley, Code 61 Ay Engineering Acoustics Academic Comittee Naval Postgraduate School Monterey, CA 93943-5000	1
5.	Instituto de Pesquisas da Marinha, Brazilian Navy 4706 Wisconsin Avenue, NW Washington, DC 20016	4
6.	Brazilian Naval Comission 4706 Wisconsin Avenue, N.W. Washington, DC 20016	4
7.	Dr. Lawrence J. Ziomek, Code 62 Zm Naval Postgraduate School Monterey, CA 93943-5000	3
8.	Dr. James H. Miller, Code 62 Mr Naval Postgraduate School Monterey, CA 90943-5000	1
9.	Dr. Marshall Orr, Code 1125 OA Office of Naval Research 800 North Quincy Street Arlington, VA 22217	1
11.	Captain Mario Agostinho de Freitas, Brazilian Navy Diretoria de Armamento e Comunicações da Marinha 4706 Wisconsin Avenue, N.W. Washington, DC 20016	2

12. CDR Ivan Pinto de Freitas, Brazilian Navy — 2
Instituto de Pesquisas da Marinha
4706 Wisconsin Avenue, N.W.
Washington, DC 20016

13. LCDR Luiz Alberto Lopes de Souza, Brazilian Navy — 2
Instituto de Pesquisas da Marinha
4706 Wisconsin Avenue, N.W.
Washington, DC 20016